

Dense vegetation promotes denudation in Patagonian rainforests

Christian H Mohr¹, Violeta Tolorza², Viktoria Georgieva³, Henry Munack⁴, Klaus M Wilcken⁵, Réka-Hajnalka Fülöp⁵, Alexandru T Codilean⁴, Eric Parra¹, and Sebastien Carretier⁶

¹University of Potsdam

²Universidad de la Frontera

³Universidad Austral de Chile

⁴University of Wollongong

⁵Australian Nuclear Science and Technology Organisation

⁶Université de Toulouse

November 23, 2022

Abstract

A geomorphological key paradigm predicts that intact forests are erosional idle, however comprise an efficient weathering machine sustaining high soil production rates. Only during times of disturbance, e.g., by earthquakes, those forests are observed to jump up to high-erosion-state, then being capable of releasing some of Earth's highest sediment yields involving massive pulses of organic carbon. Coastal temperate rainforests, in particular, do not only store unparalleled carbon stocks building up a globally important carbon sink, but are also home to high (endemic) biodiversity. Here we document extraordinarily high catchment-averaged denudation rates, across multiple disturbance cycles, under the dense vegetation of the Patagonian rainforests. There, 10 Be-derived denudation rates of $>0.8 \text{ m kyr}^{-1}$ exceed any known value from the entire Chilean Andes orogen, a highly variable $>3.000 \text{ km}$ long natural laboratory involving steep climatic and topographic gradients. We argue that such high denudation rates are consistent with a first-order control of the rainforest itself. High biomass loads exert a soil surcharge that promotes landsliding already along a relatively low critical slope angle. In contrast, denudation rates from more arid, and less forested sectors of the Chilean Andes though going along with steeper critical slope angles remain below half of our new rates derived from the Patagonian rainforests. Taken together, our study provides indication that denudation, to a higher degree than hitherto agreed on, operates as a continuous process involving soil production, vegetation, physical erosion and ecohydrological processes. Such a holistic denudational continuum, finally, is different from prevailing views that vegetation generally stabilizes hillslopes, thus promoting steep slope gradients, however, limiting landsliding activity.

1 **Dense vegetation promotes denudation in Patagonian rainforests**

2

3 **Christian H Mohr¹, Violeta Tolorza², Viktoria Georgieva³, Henry Munack⁴, Klaus M**
4 **Wilcken⁵, Réka-Hajnalka Fülöp⁵, Alexandru T Codilean⁴, Eric Parra¹ and Sebastien**
5 **Carretier⁶**

6

7 *¹University of Potsdam, Institute of Environmental Sciences and Geography, 14476 Potsdam,*
8 *Germany, cmohr@uni-potsdam, eric.parra.hormazabal@uni-potsdam.de*

9 *²Universidad de la Frontera, Department of Civil Engineering, Faculty of Engineering and*
10 *Sciences. 4811230 Temuco, Chile, violeta.tolorza@ufrontera.cl*

11 *³Universidad Austral de Chile, Institute of Physics and Mathematics, Faculty of Science, Edificio*
12 *Pugín - Campus Isla Teja, Valdivia, Chile, viktorija.georgieva@uach.cl*

13 *⁴School of Earth, Atmospheric and Life Sciences, and ARC Centre of Excellence for Australian*
14 *Biodiversity and Heritage, University of Wollongong, Wollongong, NSW 2522, Australia,*
15 *henrymunack@gmail.com, codilean@uow.edu.au*

16 *⁵Australian Nuclear Science and Technology Organisation (ANSTO), Lucas Heights, NSW 2234,*
17 *Australia, klaus.wilcken@ansto.gov.au, rekaf@ansto.gov.au*

18 *⁶Géosciences Environment Toulouse (GET), Université de Toulouse, IRD, UPS, CNRS, 31400*
19 *Toulouse, France, sebastien.carretier@get.omp.eu*

20

21 *Corresponding author: University of Potsdam, Institute of Environmental Sciences and*
22 *Geography, 14476 Potsdam, Germany, cmohr@uni-potsdam*

23 A geomorphological key paradigm predicts that intact forests are erosional idle, however
24 comprise an efficient weathering machine sustaining high soil production rates. Only
25 during times of disturbance, e.g., by earthquakes, those forests are observed to jump up to
26 high-erosion-state, then being capable of releasing some of Earth's highest sediment yields
27 involving massive pulses of organic carbon. Coastal temperate rainforests, in particular, do
28 not only store unparalleled carbon stocks building up a globally important carbon sink, but
29 are also home to high (endemic) biodiversity. Here we document extraordinarily high
30 catchment-averaged denudation rates, across multiple disturbance cycles, under the dense
31 vegetation of the Patagonian rainforests. There, ^{10}Be -derived denudation rates of $>0.8 \text{ m}$
32 kyr^{-1} exceed any known value from the entire Chilean Andes orogen, a highly variable
33 $>3.000 \text{ km}$ long natural laboratory involving steep climatic and topographic gradients. We
34 argue that such high denudation rates are consistent with a first-order control of the
35 rainforest itself. High biomass loads exert a soil surcharge that promotes landsliding
36 already along a relatively low critical slope angle. In contrast, denudation rates from more
37 arid, and less forested sectors of the Chilean Andes – though going along with steeper
38 critical slope angles – remain below half of our new rates derived from the Patagonian
39 rainforests. Taken together, our study provides indication that denudation, to a higher
40 degree than hitherto agreed on, operates as a continuous process involving soil production,
41 vegetation, physical erosion and ecohydrological processes. Such a holistic denudational
42 continuum, finally, is different from prevailing views that vegetation generally stabilizes
43 hillslopes, thus promoting steep slope gradients, however, limiting landsliding activity.

44 *Keywords:* Patagonia; Coastal Temperate Rainforest; Denudation; ^{10}Be ; Chile

45 **Forests, disturbances, and denudation**

46 Aside from regulating climate patterns¹ and accumulating carbon from the atmosphere
47 to build up important global carbon sinks², intact forests are essential to Earth's habitats because
48 they protect soils from erosion³. In turn, forest disturbance, such as deforestation, wildfires,
49 earthquakes, or windstorms promote erosion^{e.g., 4,5} by exposing bare surfaces to erosive rainfall,
50 reducing evapotranspiration, or weakening slope and river-bank stability through reduced soil
51 cohesion and root anchoring³. Yet, some of Earth's highest denudation rates, i.e., the mass removal
52 from Earth's surface by combined erosion and weathering processes, have been derived from lush
53 coastal temperate rainforests, for instance those covering the New Zealand's Southern Alps^{e.g., 4}.
54 There, steep slopes frequently fail despite sustaining dense, pristine forests gathering system-
55 relevant amounts of carbon^{5,6}, thus conditioning young landscape ages with respectively short
56 forest turnover times of these ecosystems^{e.g., 5}. High precipitation rates required to sustain dense
57 vegetation enhance denudation, potentially exceeding vegetation's anchoring effects⁷. Under
58 undisturbed conditions, however, such rainfall-denudation scaling is non-monotonic⁸⁻¹⁰ and
59 denudation rates break down after vegetation cover exceeds 50-85%⁷. Yet, quantifying
60 disturbances' long-term contribution to total denudation remains poorly documented because of
61 the annual or at most decadal focus of disturbance-related erosion studies, with a few noticeable
62 exceptions^{e.g., 11}. However, such information is not only needed to estimate the effect of single
63 disturbances on geomorphic processes^{e.g., 11}, but also to assess the functioning of forests as carbon
64 sources or sinks over hundreds to thousands of years. Leaning on the cyclic concepts of disturbance
65 ecology¹², we define long-term here as the timespan that covers multiple disturbance cycles typical
66 to the regional disturbance regime, allowing an eco-geomorphic system to recover to a pre-
67 disturbance state. As will be shown in the following, ubiquitous in situ ¹⁰Be is a particularly

68 suitable nuclide for denudation studies on such time scales^{13,14} for two reasons: First, it does not
69 integrate too long back into the past, hence justifying the strong assumption of stable vegetation
70 cover throughout the period constrained by the data. Second, despite the latter, ¹⁰Be's averaging
71 timescale still embraces multiple disturbance cycles.

72

73 **The Coastal Rainforests of Patagonia**

74 The coastal temperate rainforests (abbreviated as CTR) of Northern Patagonia form part
75 of the Valdivian Rainforest Biome, a global ecological hotspot¹⁵ ranking among the most organic
76 carbon rich biomes on Earth¹⁶. The CTRs of Northern Patagonia are marked by a cool Pacific
77 maritime, continuously wet climate (2,000 – 4,500 mm precipitation yr⁻¹)¹⁷. This climate
78 promotes dense, contiguous evergreen broadleaf forests^{17,18} that mostly consist of *Nothofagus*
79 *nitida*, *Podocarpus nubigenus*, *Drimys winterii*, *Amomyrtus meli* and *Luma apiculata*^{6,19}.

80 Following an abrupt expansion of the forest cover at around 17,800 BP²⁰, these forests generally
81 remained unchanged in composition and spatial extent at least during the last 1,000-2,000
82 years²¹. Early human occupation was intermittent and thus unlikely disturbing forests. First
83 noticeable human-made disturbances followed the arrival of European and Chilean settlers in the
84 late 19th century^{22,23} who settled mostly in the lowland given inaccessibility of higher valleys.

85 Furthermore, insect or pest-driven mortality is much less important than in drier forests²⁴.

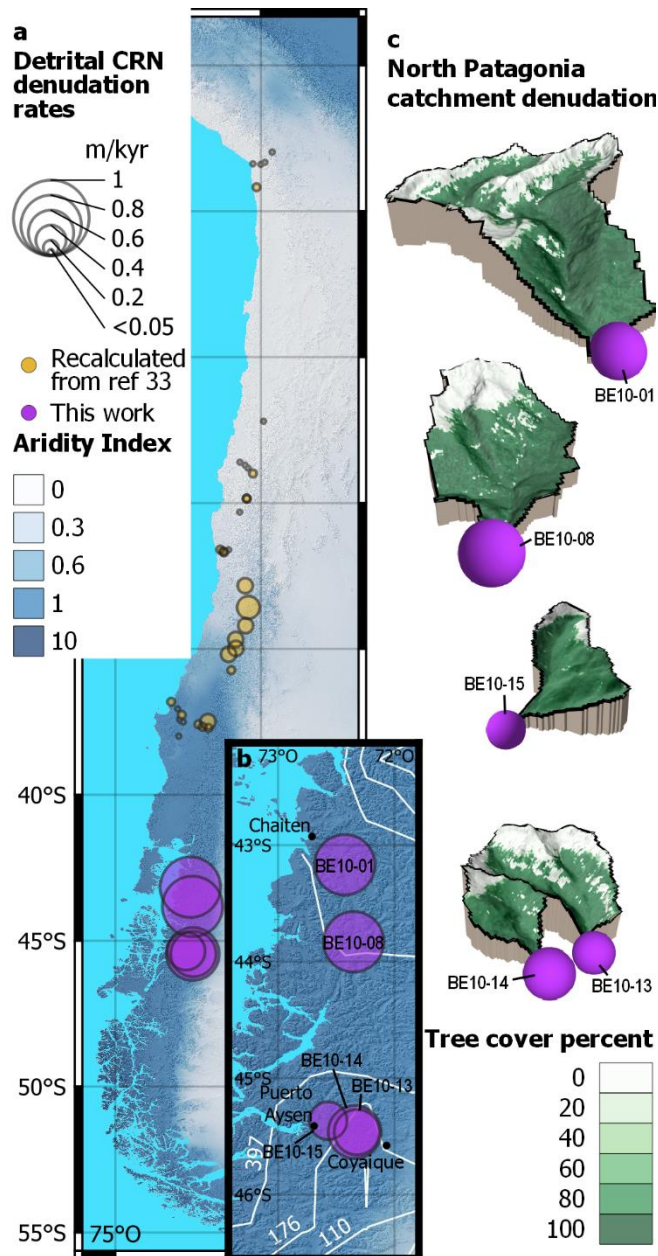
86 Relevant fire has been absent for >11,000 years^{24,25}. Instead, landslides are the prime, though
87 consequential disturbance agent^{e.g., 26,27}. Recent disturbances by earthquakes²⁸, volcanic
88 eruptions²⁹, or winds³⁰ enabled hundreds of landslides on hillslopes formerly sustaining dense
89 forest vegetation. Estimated recurrence intervals for important earthquakes and volcanic
90 eruptions (>M8 and VEI 4, respectively) are around 10² years, respectively^{6,31}. Severe

91 windstorms occur on the yearly to decadal scale^{e.g., 32}. Given said regional disturbance regime,
92 we regard ¹⁰Be as an excellent candidate as it integrates over a long enough timescale to cover
93 multiple disturbance cycles and so is suitable for looking at the effect of ‘ecological’ disturbance
94 on denudation and erosion.

95

96 **Denudation of Coastal Temperate Rainforests**

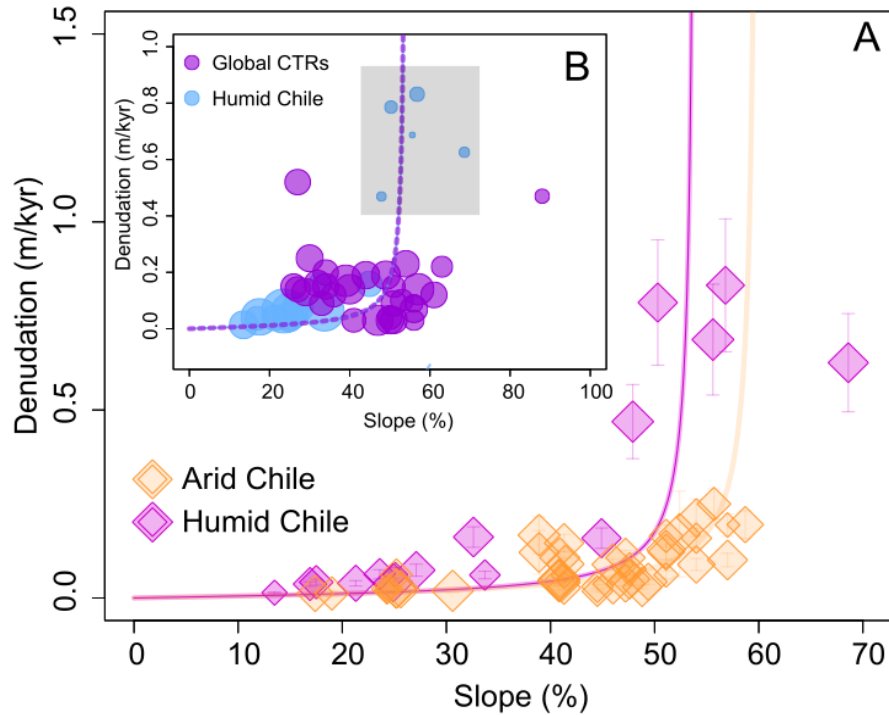
97 Here we present first ¹⁰Be denudation rate estimates for the Patagonian CTR (Figure 1).
98 We contextualize those rates using a compilation of published, recalculated catchment-wide ¹⁰Be
99 denudation rates along the Chilean Andes. With slope gradients between 50 and 70%, our study
100 catchments are relatively steep. They are underlain mostly by granitoid lithologies³³ covered by
101 soils thinner than 2m²⁹ (see also Supplementary Figure 2C), which in turn set a maximum bound
102 for shallow landslide thickness. Deeper-seated landslides involving bedrock are rare exceptions^{e.g.,}
103 ^{26,27}. Our catchments under investigation are comparable in size, i.e., 4-28 km² and do merely
104 extend into the highest elevated parts of the Andes Cordillera, thus leaving only a small part of the
105 catchments above the treeline. Despite the overall low elevation of this Andes sector, several peaks
106 exceed well above 2,500 m asl. Mean annual precipitation (MAP) and mean annual potential
107 evapotranspiration (MEP) is 1,600-2,700 mm and 630-810 mm, respectively, yielding aridity
108 indices (AI) – i.e., the ratio between MAP and MEP³⁴ – well above 1.66. From here on, we
109 distinguish between humid (AI > 1) and arid (AI < 1) conditions, respectively³⁴. The high
110 evapotranspiration rates are mainly due to the dense forest vegetation that covers large parts of all
111 studied catchments.



112

113 **Figure 1. Catchment-averaged CRN denudation rates across the Western Chilean Andes orogen. (a)**
 114 **Denudation rates in m kyr^{-1} , estimated by detrital ^{10}Be using grain size range 0.125-1.00 mm compiled**
 115 **by Ref³⁵ (yellow) and this study (purple) for the north Patagonian CTR overlaying the Aridity Index**
 116 **(AI). (b) Study area, denudation rates, and iso-lines of annual groundwater recharge in mm yr^{-1} Ref³⁶.**
 117 **(c) 2.5D-representations of studied catchments with respective denudation rates (m kyr^{-1}) and tree**
 118 **cover (%)³⁷. Bubble size scaling applies to all figures. Numbers refer to sample IDs (see**
 119 **Supplementary Table 2).**

120



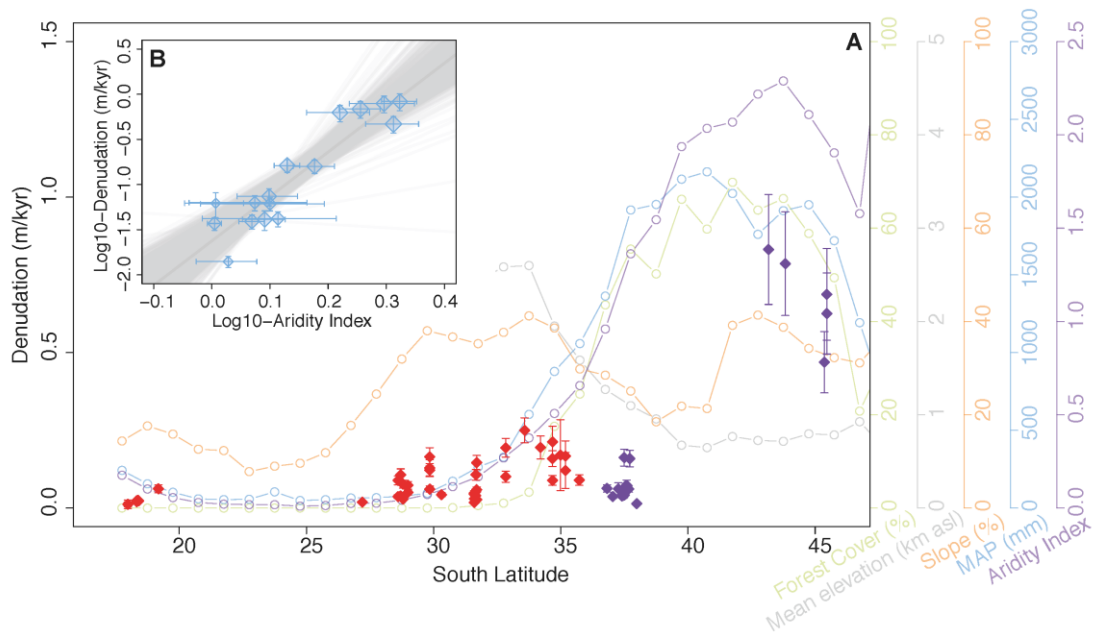
121

122 **Figure 2. Denudation rate vs slope. A: For humid (purple) and arid (orange) conditions along the**
 123 **Chilean Andes Orogen. Purple and orange lines are models⁴¹ considering 54% and 60% for critical**
 124 **slopes. Error bars refer to $\pm 1\sigma$. B: Denudation rate vs slope. The violet circles refer to compiled ¹⁰Be**
 125 **denudation rates from the OCTOPUS database³⁵ from New Zealand^{38,39} and the Pacific Northwest⁴⁰.**
 126 **The blue circles refer to humid Chile⁴²⁻⁴⁴ and our new data, that is highlighted by the grey frame.**
 127 **Circle size scales with \log_{10} of catchment size, and purple dashed line is the refers to the purple model**
 128 **in A ⁴¹.**

129

130 With up to 0.83 m kyr^{-1} (Supplementary Table 2), our new denudation rate estimates
 131 exceed any previously published rates from fluvial sands in Chile (Figure 2A, 3A). Our new
 132 denudation rates rival the maximum rates (>85-quantile) from formerly glaciated, largely forest
 133 covered landscapes with similar climate, such as New Zealand^{38,39}, and the Pacific Northwest⁴⁰
 134 (Figure 2B). Together with the Patagonian rainforest, these regions form the bulk of the global
 135 CTR Biome. Denudation rates are often reported to positively scale with precipitation under
 136 diverse climatic regimes^{e.g., 45}, but to be in negative relationship to vegetation cover⁸⁻¹⁰. Our high

137 rates, however, coincide with both the highest fractions of forest cover and highest humidity
138 along the Chilean Andean orogen (Figure 3A) where forest cover mimics MAP ($R^2=0.77$). The
139 same general pattern holds true for MAP, yet with lower predictive power, i.e., $R^2=0.52$
140 (Supplementary Figure 1). For humid conditions, AI predicts denudation rates much better than
141 precipitation ($R^2=0.84$) (Figure 3B). In this context, we recall that unlike precipitation, AI
142 recognizes evapotranspiration, and thus includes the biotic processes of root water uptake and
143 interception. In contrast, abiotic precipitation did not perform as a suitable predictor (Figure 4).
144 Consequently, we suggest AI's explanatory power for catchment-averaged denudation rates to
145 represent a positive relationship between forest cover and denudation. With 1,600-2,700 mm
146 annual precipitation⁴⁶ and annual groundwater recharge of 180-400 mm³⁶ (Figure 1B),
147 evapotranspiration in native forests (630-810 mm yr⁻¹)⁴⁷ forms an integral part of the regional
148 water balance, equaling 25-50% of the precipitation amount. Simplifying for hydrological years,
149 i.e., assuming zero interannual net changes in soil water^{e.g., 49}, the amount of evapotranspiration
150 loss is relevant for the regional hydrology. Diurnal streamflow oscillations may reflect such
151 losses in the absence of 'noise', e.g., rainfall⁴⁸. In fact, we see such diurnal cycles in catchments
152 across the Valdivian rainforest biome. AI accounts for evapotranspiration effect of the forest
153 cover on the regional hydrology which, in turn, is neglected by abiotic precipitation.
154 Consequently, our findings suggest that ecohydrological processes, such as evapotranspiration,
155 need to be accounted for when comparing denudation rates on centennial to millennial time
156 scales across biomes.



157
 158 **Figure 3. A: Denudation rates, forest cover, mean elevation, slope, mean annual precipitation**
 159 **(MAP), and aridity index (AI) along a N-S transect of the Chilean Main Cordillera. Red and violet**
 160 **squares refer to arid and humid climate, respectively. B: Scaling between denudation rates and the**
 161 **aridity index for humid climate, i.e., AI >1 ($R^2=0.84$, 10,000 Monte-Carlo simulations, $y=-$**
 162 **$1.625\pm 0.10 * 4.925\pm 0.55^x$), squares scale with NDVI (Normalized Difference Vegetation Index).**

163

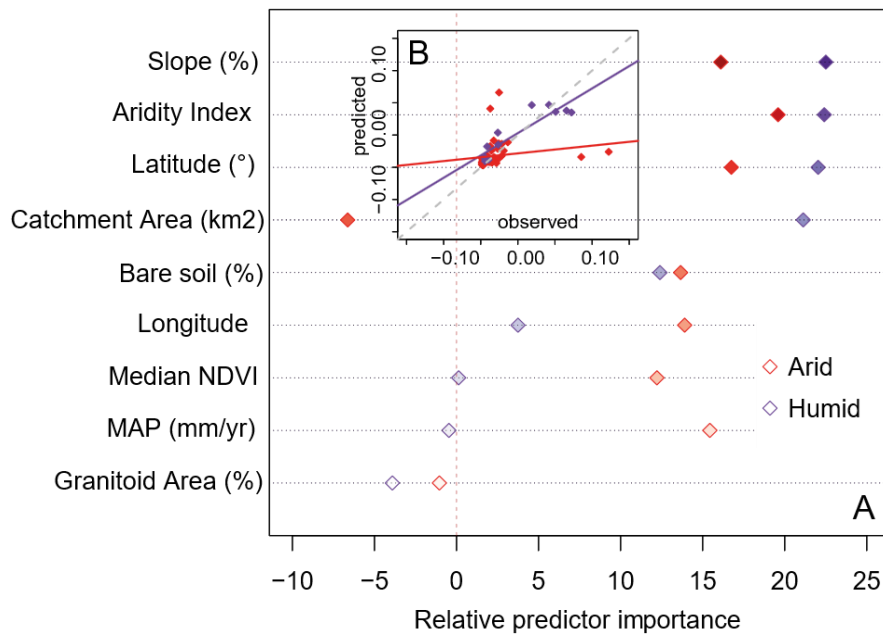
164 With 0.63 m kyr^{-1} , the catchment with highest average elevation (BE-13), is not among the
 165 fastest denuding catchments of our dataset. From this observation we infer that it is not freeze-
 166 thaw related processes, e.g., frost driven bedrock erosion⁴⁹, that is mainly recorded in our ¹⁰Be
 167 data. Instead, frequent shallow landsliding is the key erosive^{27,29,30} process in the Patagonian CTRs
 168 providing sediment to the drainage network (Supplementary Figure 2c). Hence, we conclude that
 169 supply is not limiting denudation in these forests. Instead, transport-limited fluvial erosion controls
 170 sediment export.

171 Given the rather shallow soil depths, the idea of biotic controls on denudation on centennial
 172 to millennial time scales is congruent with a lower ‘humid’ critical slope angle, i.e., 54 %,

173 compared to arid conditions (60 % (Figure 2A). Ref⁵⁰ report denudation rates increasing
174 nonlinearly with slope for the Chilean Andean Orogen. However, a lower ‘humid’ critical slope
175 angle suggests, that in the presence of vegetation, catchments are more prone to denudation for a
176 given slope gradient. This may seem counter-intuitive at first sight, because vegetation is
177 commonly considered to stabilize hillslopes by root anchoring^{e.g., 51}. How can dense vegetation
178 cause enhanced denudation?

179 With up to 1,000 Mg ha⁻¹ e.g.,^{6,47} of biomass, Patagonian CTRs are among Earth’s ‘heaviest’
180 biomes¹⁶. For a given slope gradient, such high biomass loads may be sufficient to cause failure
181 of hillslopes that would have been otherwise stable, simply driven by their own weight⁵². Cyclic
182 biomass surcharge following disturbances may lead to a tipping-bucket response to landsliding
183 largely confined into steep hilltops⁵³. Our results support the notion of hillslope failures generally
184 being constrained to steep slopes (Fig. 4). Averaged over the last 20 years without obvious
185 disturbance impairment^{27,29,30}, landslide erosion has lowered the landscape by ~ 0.4 m kyr⁻¹ (see
186 data for Huequi in Supplementary Table 3). These erosion rates are too low to exclusively explain
187 the high denudation rates within the Patagonian CTRs. From a denudational perspective, these
188 forests are apparently capable of efficiently adding to, though with the help of, mass wasting
189 effects. Weathering may benefit from vegetation as well⁷. We cannot quantify weathering rates
190 due to the lack of suitable data. However, judging from sites with comparably productive forests
191 under similar humid climates⁵⁵, we anticipate soil production rates of ≤ 0.5 mm yr⁻¹ for the
192 Patagonian CTRs. As we can then assume that rates of both erosion and soil production are largely
193 equivalent, we therefore regard the study area as largely in quasi steady state. When summing up
194 both rates, we come close to our observed denudation rates. Hence, our findings imply that
195 denudation operates as a more continuous process involving soil production, vegetation, and

196 physical erosion. Such a holistic denudational continuum, finally, is different from prevailing
 197 views that vegetation stabilizes hillslopes, leading to steep slopes with relatively little
 198 landsliding^{e.g., 54}. The higher rates we report here slightly exceed previously published exhumation
 199 rates derived from low-temperature thermochronology and constraining the record of Patagonian
 200 glaciations (5-7 Myr) along the Patagonian Andes yielding 0.2-0.7 m kyr⁻¹ Ref⁵⁶⁻⁵⁸.
 201 Thermochronology derived rates average a period, of which we can assume at most the last 16,000
 202 years as comparable to the current forest conditions^{e.g., 20}. Given the promoting effect of the forests
 203 on denudation, however, we might be looking at higher post-glacial compared to glacial
 204 denudation rates. Consistently, we may therefore treat our results to be a realistic representation of
 205 post-glacial denudation within the Patagonian CTRs but rule out depletion effects in ¹⁰Be due to a
 206 glacial heritage.



207
 208 **Figure 4. A: Relative variable importance for humid ($n=12$) and arid ($n=50$) conditions, respectively,**
 209 **for the random forest regression of ¹⁰Be denudation rates from Chile (see SI). All predictor variable**
 210 **importance was normalized to 100% (see SI), color density scales with relative importance. B:**

211 **Observed vs predicted values for standardized denudation rates for humid (purple) and arid (red)**
212 **conditions, respectively. Purple and red lines refer to linear regressions; grey dashed line refers to**
213 **the 1:1-line. We treat latitude, however, as a metric that integrates large scale climatic and**
214 **environmental conditions, thus largely mimicking AI.**

215

216 The last glaciation in the study area ceased around 17,500 BP, followed by an extensive
217 Andean deglaciation within just 1,000 years²⁰ and the fast succession of evergreen temperate
218 rainforests. Our study catchments do not extent into unvegetated high-Andean regions but sustain
219 a dense and continuous forest cover (Figure 1, Supplementary Table 1). Furthermore, we could
220 not identify any glacial heritage, such as moraine deposits, or striations. In fact, abundant boulders
221 and large grain sizes of fluvial deposits support the notion of active recent erosion within the active
222 channels of local rivers rather than reworking of glacial sediment (Supplementary Figure 2a).
223 Hence, we regard the reworking of glacial deposits as negligible, and thus consider depletion
224 effects in ¹⁰Be implausible. Our own modeling exercise to test for a possible glacial erosion
225 inheritance (Supplementary Figure 3) underpins that cosmogenic detrital ¹⁰Be records post-glacial
226 conditions in mountainous regions that were glaciated in the past.

227 Over timespans of less than 400 years, forest may stop accumulating carbon⁵⁹, though carbon
228 accumulation progressively scales with time since forest disturbance at the scale of individual
229 trees⁶⁰. These two opposing trends condition our understanding for how forest disturbances may
230 distribute broad-scale carbon stocks within each single pool of the carbon cycle. An active
231 disturbance regime promotes carbon export on time scales that may comprise multiple disturbance
232 events⁶¹. Given the minimal impact of human activity across the Patagonian rainforests, a primary
233 production rate of around 600 gC m⁻² yr⁻¹ ^{Ref6} and denudation rates averaged over 720-1,300 years,
234 our study provides a benchmark to assess modern denudation and landscape turnover rates against

235 presumably undisturbed forest conditions in one of the global hotspots for biodiversity and organic
236 carbon⁶².

237

238 **ACKNOWLEDGMENTS**

239 CHM acknowledges funding provided by DFG grant # 493703771. VT received funding by
240 postdoc grant VRIP20P001 and FONDECYT 11190864 supporting this research. EP received
241 funding from Agencia Nacional de Investigación y Desarrollo, Chile (ANID) and the
242 German Academic Exchange Service, Germany (DAAD). HM benefited from an Endeavour
243 Research Fellowship (#5547-2016) granted by the Australian Government. VG received funding
244 by an ANID/FONDECYT Postdoctoral Grant 2020 °N3200375. Drone footage for SI figure 5 was
245 acquired and provided by Benjamin Sotomayor. The authors acknowledge support from the Center
246 for Accelerator Science at Australian Nuclear Science and Technology Organisation (ANSTO)
247 through the National Collaborative Research Infrastructure Strategy (NCRIS).

248

249 **REFERENCES CITED**

- 250 1. Bonan, G. B. Forests and Climate Change: Forcings, Feedbacks, and the Climate Benefits
251 of Forests. *Science (1979)* **320**, 1444–1449 (2008).
- 252 2. Canadell, J. G. & Raupach, M. R. Managing forests for climate change mitigation. *Science*
253 *(1979)* **320**, 1456–1457 (2008).
- 254 3. Sidle, R. C. & Ochiai, H. Land Use and Global Change. in *Landslides: Processes,*
255 *Prediction, and Land Use* 1–76 (2006).
- 256 4. Korup, O., McSaveney, M. J. & Davies, T. R. H. Sediment generation and delivery from
257 large historic landslides in the Southern Alps, New Zealand. *Geomorphology* **61**, 189–207
258 (2004).
- 259 5. Hilton, R. G., Meunier, P., Hovius, N., Bellingham, P. J. & Galy, A. Landslide impact on
260 organic carbon cycling in a temperate montane forest. *Earth Surface Processes and*
261 *Landforms* **36**, 1670–1679 (2011).
- 262 6. Mohr, C. H., Korup, O., Ulloa, H. & Iroumé, A. Pyroclastic Eruption Boosts Organic
263 Carbon Fluxes Into Patagonian Fjords. *Global Biogeochemical Cycles* **31**, 1626–1638
264 (2017).

- 265 7. Starke, J., Ehlers, T. A. & Schaller, M. Latitudinal effect of vegetation on erosion rates
266 identified along western South America. *Science (1979)* **367**, 1358–1361 (2020).
- 267 8. Langbein, W. B. & Schumm, S. A. Yield of sediment in relation to mean annual
268 precipitation. *Transactions, American Geophysical Union* **39**, 1076 (1958).
- 269 9. Acosta, V. T. *et al.* Effect of vegetation cover on millennial-scale landscape denudation
270 rates in East Africa. *Lithosphere* **7**, 408–420 (2015).
- 271 10. Schmid, M., Ehlers, T. A., Werner, C., Hickler, T. & Fuentes-Espoz, J. P. Effect of
272 changing vegetation and precipitation on denudation - Part 2: Predicted landscape
273 response to transient climate and vegetation cover over millennial to million-year
274 timescales. *Earth Surface Dynamics* **6**, 859–881 (2018).
- 275 11. Vanacker, V. *et al.* Restoring dense vegetation can slow mountain erosion to near natural
276 benchmark levels. *Geology* **35**, 303 (2007).
- 277 12. Turner, M. G., Romme, W. H., Gardner, R. H., O’neill, R. v & Kratz, T. K. *A revised*
278 *concept of landscape equilibrium: Disturbance and stability on scaled landscapes.*
279 *Landscape Ecology* vol. 8 (1993).
- 280 13. Granger, D. E. & Schaller, M. Cosmogenic Nuclides and Erosion at the Watershed Scale.
281 *Elements* **10**, 369–373 (2014).
- 282 14. Schaefer, J. M. *et al.* Cosmogenic nuclide techniques. *Nature Reviews Methods Primers* **2**,
283 18 (2022).
- 284 15. Myers, N., Mittermeier, R. A., Mittermeier, C. G., da Fonseca, G. A. B. & Kent, J.
285 Biodiversity hotspots for conservation priorities. *Nature* **403**, 853–858 (2000).
- 286 16. Keith, H., Mackey, B. G. & Lindenmayer, D. B. Re-evaluation of forest biomass carbon
287 stocks and lessons from the world’s most carbon-dense forests. *Proc Natl Acad Sci U S A*
288 **106**, 11635–11640 (2009).
- 289 17. DellaSala, D. A. *Temperate and Boreal Rainforests of the World: Ecology and*
290 *Conservation.* (Island Press/Center for Resource Economics, 2011). doi:10.5822/978-1-
291 61091-008-8.
- 292 18. Alaback, P. Comparative ecology of temperate rainforests of the Americas along
293 analogous climatic gradients. *Revista Chilena de Historia Natural* **64**, 399–412 (1991).
- 294 19. de La Barrera, F., Reyes-Paecke, S. & Meza, L. Landscape analysis for rapid ecological
295 assessment of relocation alternatives for a devastated city. *Revista Chilena de Historia*
296 *Natural* **84**, 181–194 (2011).
- 297 20. Moreno, P. I. *et al.* Radiocarbon chronology of the last glacial maximum and its
298 termination in northwestern Patagonia. *Quaternary Science Reviews* **122**, 233–249 (2015).
- 299 21. de Porras, M. E. *et al.* Postglacial vegetation, fire and climate dynamics at Central Chilean
300 Patagonia (Lake Shaman, 44°S). *Quaternary Science Reviews* **50**, 71–85 (2012).
- 301 22. Torrejón, F., Cisternas, M., Alvial, I. & Torres, L. Colonial timber felling consequences of
302 the alerce forests in Chiloé, southern Chile (18th and 19th centuries). *Magallania (Punta*
303 *Arenas)* **39**, 75–95 (2011).
- 304 23. Urbina, M. X. Análisis histórico-cultural del alerce en la Patagonia septentrional
305 occidental, Chiloé, siglos XVI al XIX. *Magallania (Punta Arenas)* **39**, 57–73 (2011).
- 306 24. Buma, B. *et al.* Emergent freeze and fire disturbance dynamics in temperate rainforests.
307 *Austral Ecology* **44**, 812–826 (2019).
- 308 25. Markgraf, V. & Huber, U. M. Late and postglacial vegetation and fire history in Southern
309 Patagonia and Tierra del Fuego. *Palaeogeography, Palaeoclimatology, Palaeoecology*
310 **297**, 351–366 (2010).

- 311 26. Sommerfeld, A. *et al.* Patterns and drivers of recent disturbances across the temperate
312 forest biome. *Nature Communications* **9**, (2018).
- 313 27. Morales, B. *et al.* A comparative machine learning approach to identify landslide
314 triggering factors in northern Chilean Patagonia. *Landslides* **18**, 2767–2784 (2021).
- 315 28. Sepúlveda, S. A., Serey, A., Lara, M., Pavez, A. & Rebolledo, S. Landslides induced by
316 the April 2007 Aysén fjord earthquake, Chilean Patagonia. *Landslides* **7**, 483–492 (2010).
- 317 29. Korup, O., Seidemann, J. & Mohr, C. H. Increased landslide activity on forested hillslopes
318 following two recent volcanic eruptions in Chile. *Nature Geoscience* **2–8** (2019)
319 doi:10.1038/s41561-019-0315-9.
- 320 30. Parra, E., Mohr, C. & Korup, O. Predicting Patagonian Landslides: Roles of Forest Cover
321 and Wind Speed. (2021) doi:10.1029/2021GL095224.
- 322 31. Mohr, C. H., Manga, M., Wang, C. Y. & Korup, O. Regional changes in streamflow after
323 a megathrust earthquake. *Earth and Planetary Science Letters* **458**, 418–428 (2017).
- 324 32. Veblen, T. Forest development in tree-fall gaps in the temperate rain forest of Chile. *Natl.*
325 *Geogr. Res.* **1**, 162–183 (1985).
- 326 33. Sernageomin. Mapa geológico de Chile: versión digital. *Publicación Geología Digital* vol.
327 4 25 (2003).
- 328 34. Zomer, R. J. *et al.* *Trees and Water: Smallholder Agroforestry on Irrigated Lands in*
329 *Northern India. IWMI report* (2007).
- 330 35. Codilean, A. T. *et al.* OCTOPUS: an open cosmogenic isotope and luminescence
331 database. *Earth System Science Data* **10**, 2123–2139 (2018).
- 332 36. Müller Schmied, H. *et al.* Sensitivity of simulated global-scale freshwater fluxes and
333 storages to input data, hydrological model structure, human water use and calibration.
334 *Hydrology and Earth System Sciences* **18**, 3511–3538 (2014).
- 335 37. Hansen, M. C. *et al.* High-Resolution Global Maps of 21st-Century Forest Cover Change.
336 *Science (1979)* **342**, 850–853 (2013).
- 337 38. Burdis, A. J. Denudation rates derived from spatially-averaged cosmogenic nuclide
338 analysis in Nelson/Tasman catchments, South Island, New Zealand. (Victoria University
339 of Wellington, 2014).
- 340 39. Bellingham, M. F. Climatic effects on rapid chemical and physical denudation rates
341 measured with cosmogenic nuclides in the Ōhau catchment, New Zealand. (Victoria
342 University of Wellington, 2020).
- 343 40. Moon, S. *et al.* Climatic control of denudation in the deglaciated landscape of the
344 Washington Cascades. *Nature Geoscience* **4**, 469–473 (2011).
- 345 41. Roering, J. J., Perron, J. T. & Kirchner, J. W. Functional relationships between denudation
346 and hillslope form and relief. *Earth and Planetary Science Letters* **264**, 245–258 (2007).
- 347 42. Carretier, S. *et al.* Erosion in the Chilean Andes between 27°S and 39°S: tectonic, climatic
348 and geomorphic control. *Geological Society, London, Special Publications* **399**, 401–418
349 (2015).
- 350 43. Carretier, S. *et al.* Differences in ¹⁰Be concentrations between river sand, gravel and
351 pebbles along the western side of the central Andes. *Quaternary Geochronology* **27**, 33–
352 51 (2015).
- 353 44. Tolorza, V. Magnitude and Dynamics of catchment erosion in the Biobío River Basin.
354 (Universidad de Chile, 2015).
- 355 45. Mishra, A. K., Placzek, C. & Jones, R. Coupled influence of precipitation and vegetation
356 on millennial-scale erosion rates derived from ¹⁰Be. *PLOS ONE* **14**, e0211325 (2019).

- 357 46. Alvarez-Garretón, C. *et al.* The CAMELS-CL dataset: catchment attributes and
358 meteorology for large sample studies – Chile dataset. *Hydrology and Earth System*
359 *Sciences Discussions* 1–40 (2018) doi:10.5194/hess-2018-23.
- 360 47. Urrutia-Jalabert, R., Malhi, Y. & Lara, A. The Oldest, Slowest Rainforests in the World?
361 Massive Biomass and Slow Carbon Dynamics of Fitzroya cupressoides Temperate Forests
362 in Southern Chile. *PLOS ONE* **10**, e0137569 (2015).
- 363 48. Mohr, C. H., Manga, M., Wang, C., Kirchner, J. W. & Bronstert, A. Shaking water out of
364 soil. *Geology* **43**, 207–210 (2015).
- 365 49. Hales, T. C. & Roering, J. J. Climatic controls on frost cracking and implications for the
366 evolution of bedrock landscapes. *Journal of Geophysical Research* **112**, F02033 (2007).
- 367 50. Carretier, S. *et al.* Slope and climate variability control of erosion in the Andes of central
368 Chile. *Geology* **41**, 195–198 (2013).
- 369 51. Sidle, R. C. A Conceptual Model of Changes in Root Cohesion in Response to Vegetation
370 Management. *Journal of Environmental Quality* **20**, 43–52 (1991).
- 371 52. Vorpahl, P., Dislich, C., Elsenbeer, H., Märker, M. & Schröder, B. Biotic controls on
372 shallow translational landslides. *Earth Surface Processes and Landforms* **38**, 198–212
373 (2013).
- 374 53. Spors, S. Suicidal forests ? – Modelling biomass surcharge as a potential landslide driver
375 in temperate rainforests of Chilean Patagonia. (Universität Potsdam, 2021).
- 376 54. Larsen, I. J., Montgomery, D. R. & Korup, O. Landslide erosion controlled by hillslope
377 material. *Nature Geoscience* **3**, 247–251 (2010).
- 378 55. Amundson, R., Heimsath, A., Owen, J., Yoo, K. & Dietrich, W. E. Hillslope soils and
379 vegetation. *Geomorphology* **234**, 122–132 (2015).
- 380 56. Fosdick, J. C., Grove, M., Hourigan, J. K. & Calderón, M. Retroarc deformation and
381 exhumation near the end of the Andes, southern Patagonia. *Earth and Planetary Science*
382 *Letters* **361**, 504–517 (2013).
- 383 57. Andrić-Tomašević, N. *et al.* Quantifying Tectonic and Glacial Controls on Topography in
384 the Patagonian Andes (46.5°S) From Integrated Thermochronometry and Thermo-
385 Kinematic Modeling. *Journal of Geophysical Research: Earth Surface* **126**, (2021).
- 386 58. Georgieva, V. *et al.* Tectonic control on rock uplift, exhumation, and topography above an
387 oceanic ridge collision: Southern Patagonian Andes (47°S), Chile. *Tectonics* **35**, 1317–
388 1341 (2016).
- 389 59. Gray, A. N., Whittier, T. R. & Harmon, M. E. Carbon stocks and accumulation rates in
390 Pacific Northwest forests: Role of stand age, plant community, and productivity.
391 *Ecosphere* **7**, 1–19 (2016).
- 392 60. Stephenson, N. L. *et al.* Rate of tree carbon accumulation increases continuously with tree
393 size. *Nature* **507**, 90–93 (2014).
- 394 61. Frith, N. v. *et al.* Carbon export from mountain forests enhanced by earthquake-triggered
395 landslides over millennia. *Nature Geoscience* **11**, 772–776 (2018).
- 396 62. Smith, R. W., Bianchi, T. S., Allison, M., Savage, C. & Galy, V. High rates of organic
397 carbon burial in fjord sediments globally. *Nature Geoscience* **8**, 450–453 (2015).
- 398 63. Singer, B. S., Ackert, R. P. & Guillou, H. 40Ar/39Ar and K-Ar chronology of Pleistocene
399 glaciations in Patagonia. *Geological Society of America Bulletin* **116**, 434 (2004).
- 400 64. Cembrano, J., Hervé, F. & Lavenu, A. The Liquiñe Ofqui fault zone: a long-lived intra-arc
401 fault system in southern Chile. *Tectonophysics* **259**, 55–66 (1996).

- 402 65. Pepin, E., Carretier, S., Guyot, J. L. & Escobar, F. Specific suspended sediment yields of
403 the Andean rivers of Chile and their relationship to climate, slope and vegetation.
404 *Hydrological Sciences Journal* **55**, 1190–1205 (2010).
- 405 66. Carretier, S. *et al.* Review of erosion dynamics along the major N-S climatic gradient in
406 Chile and perspectives. *Geomorphology* **300**, 45–68 (2018).
- 407 67. Lal, D. Cosmic ray labeling of erosion surfaces: in situ nuclide production rates and
408 erosion models. *Earth and Planetary Science Letters* **104**, 424–439 (1991).
- 409 68. von Blanckenburg, F. & Willenbring, J. K. Cosmogenic Nuclides: Dates and Rates of
410 Earth-Surface Change. *Elements* **10**, 341–346 (2014).
- 411 69. Kohl, C. P. & Nishiizumi, K. Chemical isolation of quartz for measurement of in-situ -
412 produced cosmogenic nuclides. *Geochimica et Cosmochimica Acta* **56**, 3583–3587 (1992).
- 413 70. von Blanckenburg, F., Belshaw, N. S. & O’Nions, R. K. Separation of ⁹Be and
414 cosmogenic ¹⁰Be from environmental materials and SIMS isotope dilution analysis.
415 *Chemical Geology* **129**, 93–99 (1996).
- 416 71. Wilcken, K. M. *et al.* SIRIUS Performance: ¹⁰Be, ²⁶Al and ³⁶Cl measurements at
417 ANSTO. *Nuclear Instruments and Methods in Physics Research Section B: Beam
418 Interactions with Materials and Atoms* **455**, 300–304 (2019).
- 419 72. Nishiizumi, K. *et al.* Absolute calibration of ¹⁰Be AMS standards. *Nuclear Instruments
420 and Methods in Physics Research, Section B: Beam Interactions with Materials and
421 Atoms* **258**, 403–413 (2007).
- 422 73. Mudd, S. M., Harel, M.-A., Hurst, M. D., Grieve, S. W. D. & Marrero, S. M. The CAIRN
423 method: automated, reproducible calculation of catchment-averaged denudation rates from
424 cosmogenic nuclide concentrations. *Earth Surface Dynamics* **4**, 655–674 (2016).
- 425 74. Braucher, R., Merchel, S., Borgomano, J. & Bourlès, D. L. Production of cosmogenic
426 radionuclides at great depth: A multi element approach. *Earth and Planetary Science
427 Letters* **309**, 1–9 (2011).
- 428 75. Jarvis, A., Reuter, H. I., Nelson, A. & Guevara, E. Hole-filled SRTM for the globe
429 Version 4. *available from the CGIAR-CSI SRTM 90m Database* vol. 15
430 <http://srtm.csi.cgiar.org> (2008).
- 431 76. Stone, J. O. Air pressure and cosmogenic isotope production. *Journal of Geophysical
432 Research: Solid Earth* **105**, 23753–23759 (2000).
- 433 77. Compo, G. P. *et al.* The Twentieth Century Reanalysis Project. *Quarterly Journal of the
434 Royal Meteorological Society* vol. 137 1–28 (2011).
- 435 78. Codilean, A. T. Calculation of the cosmogenic nuclide production topographic shielding
436 scaling factor for large areas using DEMs. *Earth Surface Processes and Landforms* **31**,
437 785–794 (2006).
- 438 79. Zambrano-Bigiarini, M., Nauditt, A., Birkel, C., Verbist, K. & Ribbe, L. Temporal and
439 spatial evaluation of satellite-based rainfall estimates across the complex topographical
440 and climatic gradients of Chile. *Hydrology and Earth System Sciences* **21**, 1295–1320
441 (2017).
- 442 80. Zhao, Y. *et al.* Detailed dynamic land cover mapping of Chile: Accuracy improvement by
443 integrating multi-temporal data. *Remote Sensing of Environment* **183**, 170–185 (2016).
- 444 81. Zomer, R. J., Trabucco, A., Bossio, D. A. & Verchot, L. v. Climate change mitigation: A
445 spatial analysis of global land suitability for clean development mechanism afforestation
446 and reforestation. *Agriculture, Ecosystems and Environment* **126**, 67–80 (2008).

- 447 82. Gorelick, N. *et al.* Google Earth Engine: Planetary-scale geospatial analysis for everyone.
448 *Remote Sensing of Environment* **202**, 18–27 (2017).
- 449 83. Breiman, L. Random Forests. *Machine Learning* **45**, 5–32 (2001).
- 450 84. Liaw, A. & Wiener, M. Classification and Regression by randomForest. *R News* **2**, 18–22
451 (2002).
- 452 85. Strobl, C., Boulesteix, A. L., Kneib, T., Augustin, T. & Zeileis, A. Conditional variable
453 importance for random forests. *BMC Bioinformatics* **9**, 1–11 (2008).
- 454 86. Larsen, I. J. *et al.* Rapid soil production and weathering in the Southern Alps, New
455 Zealand. *Science* **343**, 637–40 (2014).
- 456 87. Carretier, S. *et al.* A note on ¹⁰Be-derived mean erosion rates in catchments with
457 heterogeneous lithology: examples from the western Central Andes. *Earth Surface*
458 *Processes and Landforms* **40**, 1719–1729 (2015).
- 459 88. Kober, F. *et al.* Complex multiple cosmogenic nuclide concentration and histories in the
460 arid Rio Lluta catchment, northern Chile. *Earth Surface Processes and Landforms* **34**,
461 398–412 (2009).
- 462 89. Braucher, R. *et al.* Determination of muon attenuation lengths in depth profiles from in
463 situ produced cosmogenic nuclides. *Nuclear Instruments and Methods in Physics*
464 *Research Section B: Beam Interactions with Materials and Atoms* **294**, 484–490 (2013).
465
- 466

467 **FIGURE CAPTIONS**

468 Figure 5. Catchment-averaged CRN denudation rates across the Western Chilean Andes orogen.
469 (a) Denudation rates in m kyr^{-1} , estimated by detrital ^{10}Be using grain size range 0.125-1.00 mm
470 compiled by Ref³⁵ (yellow) and this study (purple) for the north Patagonian CTR overlaying the
471 Aridity Index (AI). (b) Study area, denudation rates, and iso-lines of annual groundwater recharge
472 in mm yr^{-1} Ref³⁶. (c) 2.5D-representations of studied catchments with respective denudation rates
473 (m kyr^{-1}) and tree cover (%)³⁷. Bubble size scaling applies to all figures. Numbers refer to sample
474 IDs (see Supplementary Table 2).

475

476 Figure 6. Denudation rate vs slope. A: For humid (purple) and arid (orange) conditions along the
477 Chilean Andes Orogen. Purple and orange lines are models⁴¹ considering 54% and 60% for critical
478 slopes. Error bars refer to $\pm 1\sigma$. B: Denudation rate vs slope. The violet circles refer to compiled
479 ^{10}Be denudation rates from the OCTOPUS database³⁵ from New Zealand^{38,39} and the Pacific
480 Northwest⁴⁰. The blue circles refer to humid Chile⁴²⁻⁴⁴ and our new data, that is highlighted by the
481 grey frame. Circle size scales with \log_{10} of catchment size, and purple dashed line is the refers to
482 the purple model in A⁴¹.

483

484 Figure 7. A: Denudation rates, forest cover, mean elevation, slope, mean annual precipitation
485 (MAP), and aridity index (AI) along a N-S transect of the Chilean Main Cordillera. Red and
486 violet squares refer to arid and humid climate, respectively. B: Scaling between denudation rates
487 and the aridity index for humid climate, i.e., $\text{AI} > 1$ ($R^2=0.84$, 10,000 Monte-Carlo simulations,
488 $y=-1.625\pm 0.10 * 4.925\pm 0.55^x$), squares scale with NDVI (Normalized Difference Vegetation
489 Index).

490 Figure 8. A: Relative variable importance for humid ($n=12$) and arid ($n=50$) conditions,
491 respectively, for the random forest regression of ^{10}Be denudation rates from Chile (see SI). All
492 predictor variable importance was normalized to 100% (see SI), color density scales with relative
493 importance. B: Observed vs predicted values for standardized denudation rates for humid (purple)
494 and arid (red) conditions, respectively. Purple and red lines refer to linear regressions; grey dashed
495 line refers to the 1:1-line. We treat latitude, however, as a metric that integrates large scale climatic
496 and environmental conditions, thus largely mimicking AI.

497 **SUPPLEMENTARY INFORMATION**

498 **Sampled Catchments**

499 The topography of Northern Chilean Patagonia is largely a product of quaternary
500 volcanism and massive glacial erosion. The latter carved deep fjords between eroded islands and
501 peninsulas, leaving behind a spectacular landscape of steep slopes and small cirques in headwaters
502 mounting above broad, flat-bottomed valleys⁶³. All catchments drain into the Pacific Ocean (see
503 as an example Supplementary Figure 5).

504 The regional tectonics are dominated by active subduction and intra-arc strike-slip motion
505 along the Southern Chile Trench and the Liquiñe-Ofqui Fault zone⁶⁴, respectively, and Quaternary
506 arc volcanism. Among them, the Chaitén, Michinmahuida and Corcovado volcanoes are prominent
507 landscape features and belong to the Andean Southern Volcanic Zone (SVZ).

508 We collected ($n = 5$) new samples of fluvial sediment in headwater catchments draining parts of
509 the Northern Chilean Patagonian Andes (43°0'-45°40'S) from north to south along a transect from
510 Chaitén township to the cities of Coyhaique and Puerto Aysén (Figure 1). Given restricted
511 accessibility due to dense forest, we sampled headwater catchments that are accessible from the
512 main roads, i.e., along the Carretera Austral. All headwaters drain into the Pacific Ocean via the
513 connecting Yelcho, Palena, of Aysén rivers. Dense coastal rainforest dominates all catchments.
514 Our sampled catchments do not extent into highest-andine regions. Such fact minimizes effects of
515 glacial and snow cover on shielding on cosmogenic-derived denudation rates.

516 Our data are the first to fill the Andean gap between 41° and 52°S. The most proximal reported
517 denudation rates, i.e., north of 41°S and south of 52°S, are at the order of $<0.2 \text{ m kyr}^{-1}$ Ref^{65,66}. Yet,
518 we regard these rates as comparable to a limited degree only. For example, rates from $\sim 52^\circ\text{S}$ based
519 on decennial sediment flux monitoring originate east from the Andean divide in the much drier

520 Pampean region⁶⁵. Likewise, comparison to exhumation rates derived from low-temperature
521 thermochronology yielding 0.2-0.7 m kyr⁻¹ along the Patagonian Andes⁵⁶⁻⁵⁸ is also limited due to
522 different time scales constrained. Thermochronology derived rates average a period, of which we
523 can assume at most the last 16,000 years as comparable to the current environmental, particularly
524 forest, conditions^{e.g., 20}.

525

526 **¹⁰Be sampling and lab procedure**

527 Secondary cosmic radiation reacts with minerals of Earth surface producing cosmogenic
528 nuclides such as ¹⁰Be, which production rates are well known for quartz⁶⁷. The production rate of
529 a mineral decreases exponentially at depth. When minerals reach a steadily ¹⁰Be concentration, it
530 scales inversely with the rate of surface removal^{67,68}. That surface removal, here called denudation,
531 involves both physical erosion and chemical weathering. The quartz present in well-mixed fluvial
532 sediments provides spatially averaged erosion rates from upstream areas, which may range from
533 single hillslopes to continental river basins¹³. The timescale for a steadily erosion rate refers to the
534 mineral residence time within the particle mean free path in rocks⁶⁷. That is, the characteristic time
535 τ necessary to erode a ~60 cm thickness strip¹³

536 Samples were prepared for cosmogenic ¹⁰Be analysis at the University of Wollongong.
537 Quartz was purified following procedures described in⁶⁹ using froth flotation to separate feldspars
538 from quartz, and Be was separated following procedures described in⁷⁰. Samples were spiked with
539 $\approx 250 \mu\text{g}$ of ⁹Be from a low-level beryl carrier solution added prior to complete HF dissolution.
540 Sample purity was assessed following dissolution in HF, with native Al concentrations in all
541 samples being $< \approx 200$ ppm (average = 168 ppm). To test for the presence of native ⁹Be in our

542 samples, we also measured the Be concentration via ICP-OES in the dissolved material, obtaining
543 concentration differences < 3%, the typical uncertainty of the method (average difference $\approx 1\%$).

544 $^{10}\text{Be}/^9\text{Be}$ ratios were measured using the 6MV SIRIUS facility at ANSTO⁷¹ and were
545 normalised to the KN-5-2, KN-5-4, and KN-6-2^{Ref72} standards. Analytical uncertainties for the
546 final ^{10}Be concentrations (atoms g^{-1}) include AMS measurement uncertainties (larger of counting
547 statistics or standard deviation of repeats and blank corrections) in quadrature with 1-2% for ^{10}Be
548 standard reproducibility (depending on the individual AMS measurement conditions) and 1%
549 uncertainty in the ^9Be carrier concentration.

550 Denudation rates were calculated using the open-source program CAIRN v.1⁷³. Basin-
551 averaged nuclide production from neutrons and muons was calculated with the approximation of⁷⁴
552 and using a sea-level and high-latitude total production rate of $4.3 \text{ atoms g}^{-1} \text{ yr}^{-1}$ Ref⁷³. Production
553 rates for catchment-wide denudation rates were calculated at every grid cell of a hydrologically
554 enforced 90 m SRTM DEM⁷⁵, using the time-independent Lal/Stone scaling scheme⁷⁶.
555 Atmospheric pressure was calculated via interpolation from the NCEP2 reanalysis data⁷⁷.
556 Topographic shielding was calculated from the same DEM using the method of⁷⁸ with $\Delta\theta = 8^\circ$ and
557 $\Delta\phi = 5^\circ$.

558 All data that we used here as for comparison reasons were obtained from the OCTOPUS
559 database³⁵ and⁶⁶. We recalculated the data of^{44,66} using the Octopus protocol. Our new data are
560 calculated in the same way. The differences from all recalculated and original data^{44,66} were minor,
561 i.e. the ratio was 0.969 ± 0.112 (see Supplementary Table 4).

562

563 **GIS-computations**

564 We ran all spatial computations to calculate catchment-wide covariates in QGIS 3.2.2, GRASS
565 7.8.2 and SAGA 2.3.2. To this end we derived topographic metrics such as elevation and local
566 slope from SRTM digital elevation models, i.e. 30 and 90m ground resolution⁷⁵ to both broadly
567 characterize the topography and also being consistent with the OCTOPUS data. We extracted
568 catchment-wide mean annual precipitation from the CHIRPS v2 product evaluated for Chile by⁷⁹
569 the tree cover percent from³⁷, the bare surfaces from⁸⁰ and the aridity^{34,81}. The latter can be
570 expressed by the dimensionless Aridity Index (AI) that is defined as

$$AI = \frac{MAP(mm)}{MAE(mm)} \quad (\text{eq. 1})$$

571 where MAP refers to mean annual precipitation and MAE to mean annual potential
572 evapotranspiration. MAE is calculated using the Hargreaves model and validated using n = 2288
573 Penman-Monteith values at climate stations in South America (and Africa)⁸¹. We estimated
574 spectral indices such as NDVI within each catchment using Google Earth Engine⁸². Mean NDVI
575 was computed on COPERNICUS/S2_SR collection of January 2021 with less than 20% of cloudy
576 pixel percentage ([https://developers.google.com/earth-engine/datasets/catalog/
577 COPERNICUS_S2_SR#description](https://developers.google.com/earth-engine/datasets/catalog/COPERNICUS_S2_SR#description)).

578

579 **Calculation of landslide erosion rates**

580 We used the landslide inventories of³⁰ who approximated the total affected area for each
581 landslide, that is source, runout, and deposition zones. We used the landslide area and calculated
582 the volume of the eroded material by assigning a maximum depth of the landslide slide plane of
583 2m consistent with²⁹, who measured the geometry of landslides around Chaitén volcano from
584 photogrammetric unmanned aerial vehicle (UAV) surveys and randomly confirmed landslide scar

585 and deposit depth using measuring tape and an inclinometer. At none of these sites did we find
586 deposits thicker than about 2 m.

587 Next, we averaged the calculated landslide volume (L^3) across the area(s) (L^2). The total
588 area of Huequi peninsula is 897 km², Chaitén (2,413 km²), and Calbuco (4,750 km²)³⁰. Lastly, we
589 divided calculated height (L, here as m) by the period (20 years) covered by the landslide
590 inventory. We approximated the date of landslide occurrence at annual precision judging from the
591 timestamps of image pairs showing the latest undisturbed conditions and the earliest landslide
592 occurrence. We recorded 411 landslides (total landslide area: 32.7 km²) during 2001-2019 for
593 Calbuco, 616 landslides (total landslide area: 19.4 km²) during 2001-2019, and 38 landslides for
594 Huequi (total landslide area: 3.4 km²) during 2001-2019. The results are shown in Supplementary
595 Table 3.

596

597 **Data Analysis on denudation rates**

598 We used Random Forest regression⁸³ to identify the most relevant topographic, climatic,
599 and disturbance-related controls on the denudation rates for Chile (see Supplementary Table 1).
600 Random forests (RF) are ensembles of decision trees trained on data, forming a robust
601 nonparametric model capable of handling large nonlinear, noisy, fragmented, or correlated
602 multidimensional data for classification^{84,85}, and combine bootstrap aggregating with random
603 variable selection⁸³. The strategy is to explore the importance of predictors using bootstrapped data
604 and predictor subsets for growing decision trees. Our response variable refers to the erosion rates
605 (mm/year). Predictor variables include continuous data on hydro-climatology, geology, land cover
606 and topography. We grew random forests with 10,000 individual trees, setting the number of
607 variables at each node to 2 (out of a total of 9 predictors, see Figure 4). We assessed relative

608 variable importance for a random forest regression of ^{10}Be denudation rates. To this end, we
609 normalized all predictor variable importance to 100%. We employ Random Forest (RF) statistics
610 to quantify controls for the observed erosion rates. Our RF-model fit was good for humid
611 conditions, but poor for arid conditions ($R^2=0.62$ vs $R^2=0.06$).

612 We calculated the critical slope following ⁴⁹ using ordinary least square modeling fitting
613 for humid ($\text{AI}>1$) and arid ($\text{AI}<1$) subsets of our data compilation for the Chilean Andes orogen.

614 Comparing to other similar landscapes, we excluded data from Hopkins and Dobson valley,
615 NZ, ³⁹ that are locally affected by deep-seated landslides, thus comprise a different process domain.
616 We also excluded the work by ⁸⁶ as these catchments are dominated by shrublands and/or extend
617 into high-alpine terrain⁸⁶ in contrast to our catchments.

618

619 **Supplementary Table**

620 Supplementary Table 1. Properties of studied catchments. Slope and elevation come from 90m
 621 SRTM data⁷⁵, MAP from satellite-based rainfall product CHIRPS 1981-2016^{Ref79}, AI comes
 622 from^{34,81} from, forest cover from³⁷, and fraction of granitic lithology with respect to total
 623 catchment area from³³. Uncertainty is given as $\pm 1\sigma$.

Sample ID	BE10-01	BE10-08	BE10-13	BE10-14	BE10-15
Lat (°)	-43.1676	-43.8284	-45.4609	-45.4593	-45.3626
Lon (°)	-72.4277	-72.3521	-72.3238	-72.3426	-72.5708
Slope (%)	58.2 \pm 28.1	51.6 \pm 25.6	70.5 \pm 32.5	57.1 \pm 28.4	49.9 \pm 25.3
Catchment (km2)	28.44	18.00	10.81	4.09	8.53
MAP (mm)	2528	2703	1635	1731	2513
Elevation (m asl)	921 \pm 308	838 \pm 473	983 \pm 315	823 \pm 288	866 \pm 274
AIMedian	2.06	2.02	1.66	1.79	2.04
Forest cover (%)	60.8	69.5	52.5	72.3	76.7
Granitic (%)	40.2	96	100	99.1	97.9

624

625

626 Supplementary Table 2. Summary of cosmogenic ^{10}Be measurements and calculated denudation, uncertainty is given as $\pm 1\sigma$

627

Sample ID	UOW Sample ID	ANSTO Cathode ID	Total Qtz (g)	^9Be Spike (μg)	^{27}Al ICP ($\mu\text{g}\cdot\text{g}^{-1}$)	^9Be ICP (μg)	%Diff $^9\text{Be}^{(a)}$	$^{10}\text{Be}/^9\text{Be}^{(b,c)}$ (10^{-15})	$^{10}\text{Be}^{(c)}$ ($\text{atoms}\cdot\text{g}^{-1}$)	CAIRN Total Scaling Factor	Erosion Rate $^{(c)}$ ($\text{mm}\cdot\text{yr}^{-1}$)	Averaging Timescale (kyr)
BE-10-1	UOW001	Be829	40.160	263.9	203.9	257.6	2.43	16.90 ± 0.94	7421 ± 443	2.13	0.83 ± 0.18	0.7
BE-10-8	UOW002	Be830	39.985	261.5	173.9	261.8	0.11	18.11 ± 1.00	7912 ± 471	2.14	0.79 ± 0.17	0.8
BE-10-13	UOW003	Be831	40.367	261.9	144.6	262.2	0.10	24.49 ± 1.23	10618 ± 584	2.31	0.63 ± 0.13	1.0
BE-10-14	UOW004	Be832	40.118	261.5	189.7	263.2	0.67	19.76 ± 1.13	8604 ± 527	2.03	0.69 ± 0.15	0.9
BE-10-15	UOW005	Be833	40.236	262.3	128.4	259.3	1.17	30.28 ± 1.37	13192 ± 665	2.13	0.47 ± 0.10	1.3

a) difference between ^9Be spike added and ^9Be measured in dissolved sample via ICP-OESb) corrected using a procedural blank with $^{10}\text{Be}/^9\text{Be} = 0.483 \pm 0.165 \times 10^{-15}$ (n=5)

c) uncertainties at 1-sigma level

628

629

630 Supplementary Table 3. Landslide erosion rates estimated for three areas within the CTR of
 631 northern Patagonia: 1) Calbuco area (affected by the Calbuco eruption in 2015; 2) Huequi area
 632 (without relevant human or natural disturbances and used as representing undisturbed state); 3)
 633 Chaitén area where rainforest stand in various states of post-volcanic disturbance following the
 634 2008 Chaiten eruption.

635

Study area	Reference coordinates		Total volume (km ³)	Landslide erosion (m kyr ⁻¹)
	Lat (°)	Long (°)		
Calbuco	-41.1917	-72.4909	0.06542	0.72
Huequi	-42.3680	-72.5919	0.00678	0.39
Chaiten	-42.7799	-72.5222	0.03882	0.84

636

637

638

639 Supplementary Table 4. New and compiled ⁶⁶ data of detrital ¹⁰Be concentration and denudation rates for samples of grain size

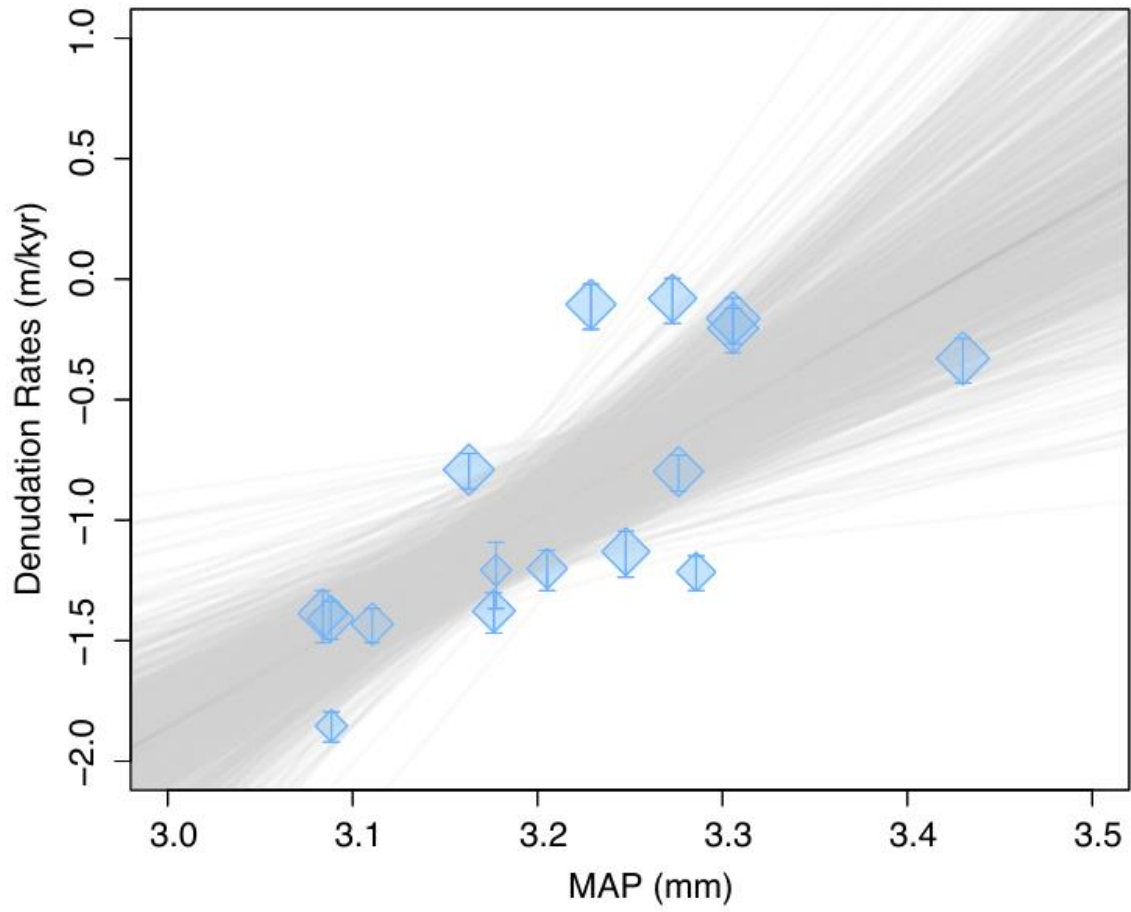
640 between 0.126-1 mm within Chilean Western Andes. * Denudation rates recalculated for Octopus database in this work.

Name and reference	Cosmogenic Nuclide Concentration (at/g) Carretier et al. 2018	Cosmogenic Nuclide Concentration uncertainty (at/g) Carretier et al 2018	Cosmogenic Nuclide Concentration (at/g) Octopus	Cosmogenic Nuclide Concentration uncertainty (at/g) Octopus	Denudation rate (mm/a) Carretier et al 2018	Denudation rate uncertainty (mm/a) Carretier et al 2018	Denudation rate (mm/a) Octopus	Denudation rate uncertainty (mm/a) Octopus
BE10-01			7421*	443*			0.831*	0.177*
BE10-08			7912*	471*			0.786*	0.167*
BE10-13			10618*	584*			0.626*	0.131*
BE10-14			8604*	527*			0.687*	0.147*
BE10-15			13192*	665*			0.469*	0.098*
MAU1 ⁵⁰	129351	14825	129351	7413	0.090	0.017	0.102	0.020
LON1 ⁵⁰	64381	29145	64381	14573	0.121	0.058	0.175	0.053
TEN1 ⁵⁰	73331	48099	73331	24050	0.170	0.114	0.163	0.067
TIN1 ⁵⁰	99370	5275	99370	2638	0.159	0.025	0.163	0.030
CAC1 ⁵⁰	91404	10713	91404	5357	0.195	0.037	0.194	0.037
MAI1 ⁵⁰	87032	5010	87032	2505	0.250	0.040	0.257	0.047
ACO1 ⁵⁰	101191	2915	101191	1458	0.194	0.030	0.211	0.038
CHO1 ⁵⁰	195648	6708	195648	3354	0.059	0.009	0.067	0.012
CHO0820 ⁵⁰	234948	10795	234948	5398	0.040	0.006	0.047	0.009
CHO0822S ⁵⁰	198207	5803	198207	2902	0.053	0.008	0.061	0.012
CHO0823S ⁵⁰	218067	9450	218067	4725	0.048	0.008	0.055	0.010
ILL1 ⁵⁰	468966	13507	468966	6754	0.030	0.005	0.031	0.006
HUR1 ⁵⁰	593076	38635	593076	19318	0.043	0.007	0.036	0.007
ELK1 ⁵⁰	177039	23322	177039	11661	0.129	0.026	0.149	0.029
ELK2 ⁵⁰	186943	16714	186943	8357	0.122	0.021	0.141	0.026
HUA1 ⁵⁰	479983	13641	479983	6821	0.050	0.008	0.052	0.009
HUA7 ⁵⁰	833051	53481	833100	53500	0.029	0.005	0.028	0.005
HUA10 ⁵⁰	588998	16567	589000	16600	0.039	0.006	0.038	0.007
HUA12 ⁵⁰	598649	24962	598600	25000	0.037	0.006	0.035	0.007
SAN1 ⁵⁰	1027511	153842	1027511	76921	0.019	0.004	0.017	0.003
CHIZ1 ⁸⁷	116710	17124	117000	17000	0.062	0.013	0.077	0.019

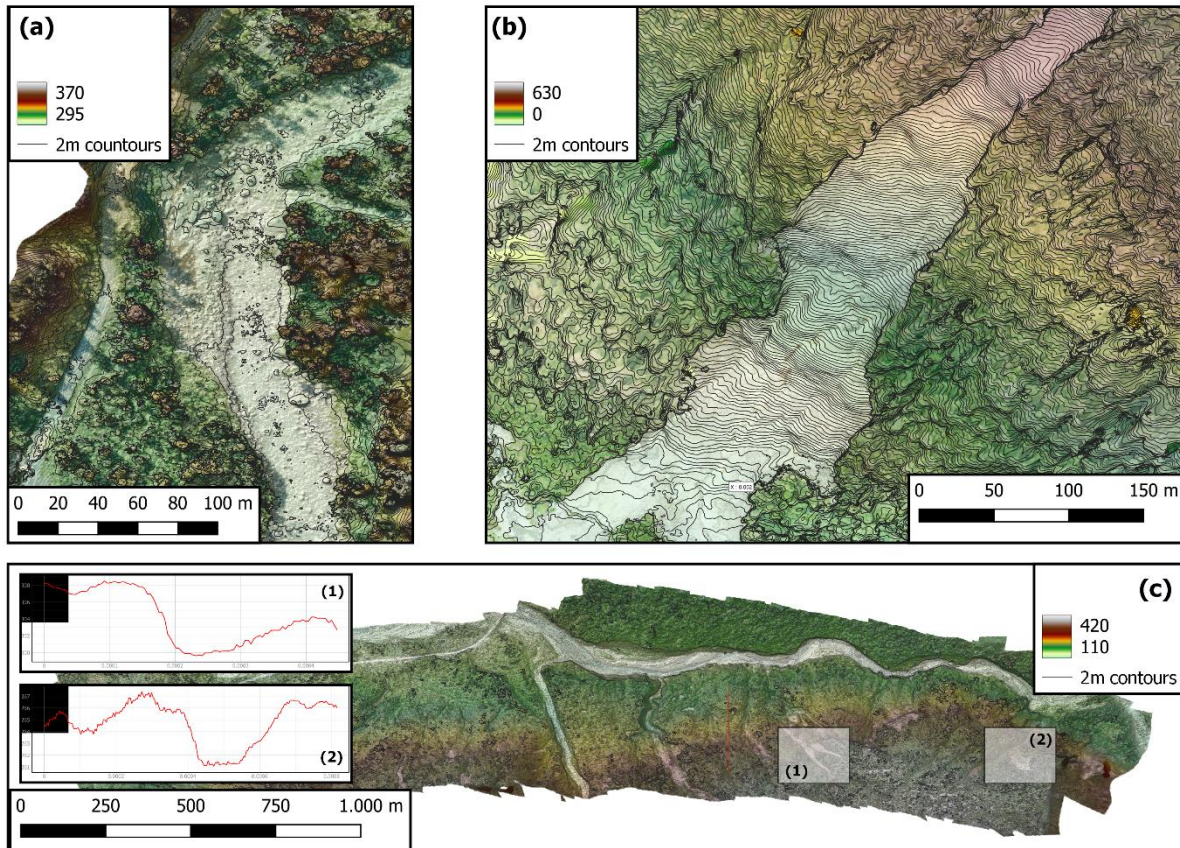
LL1 ⁸⁸	1069000	56000	1069000	56000	0.024	0.004	0.023	0.004
LL2 ⁸⁸	975000	40000	975000	40000	0.023	0.004	0.023	0.004
LL3 ⁸⁸	866000	54000	866000	54000	0.025	0.004	0.0238	0.00463
LL4 ⁸⁸	2435000	3000000	2435000	306000	0.012	0.014	0.011	0.002
LL5 ⁸⁸	2373000	1490000	2373000	149000	0.012	0.008	0.011	0.002
Bbd2-2 ^{44,66}	75957	9631	75957*	9631*	0.063	0.012	0.075*	0.018*
Bbm1-2 ⁴²	116638	9459	117000	9460	0.061	0.010	0.066	0.014
D1-1 ⁴²	86277	14037	86300	14000	0.074	0.016	0.064	0.017
C1-1b ^{44,66}	113680	20735	113680*	20735*	0.041	0.010	0.039*	0.011*
C3-2 ^{44,66}	97896	8272	97896*	8272*	0.039	0.007	0.037*	0.009*
VC1-2 ^{44,66}	95900	10529	95900*	10529*	0.042	0.008	0.042*	0.011*
LC1 ^{44,66}	89686	24690	89686*	24690*	0.062	0.019	0.073*	0.026*
Ca1 ^{44,66}	35951	2506	35951*	2506*	0.162	0.027	0.154*	0.034*
R1 ^{44,66}	252782	8226	252782*	8226*	0.014	0.002	0.013*	0.003*
H1 ^{44,66}	41242	3172	41242*	3172*	0.159	0.027	0.148*	0.032*
Mi2 ^{44,66}	93772	4280	93772*	4280*	0.037	0.006	0.035*	0.008*

641

642
643 **Supplementary Figure**



644
645 Supplementary Figure 1. Denudation rate vs MAP, log-scaled, 10,000 MC simulations, $Y = -14.951 \pm 3.40$
646 $* 4.364 \pm 1.059^X$; $R^2=0.517$. Square size scales with \log_{10} of NDVI.



647

648 Supplementary Figure 2. RGB UAV-footage. (a) of active channel of Turbio river, boulder of up

649 to 6 m edge lengths ($42^{\circ}57'16.16''\text{S}$, $72^{\circ}23'39.51''\text{W}$), (b) rare deep landslide close to Chaitén

650 township ($42^{\circ}57'1.00''\text{S}$, $72^{\circ}38'37.88''\text{W}$), (c) shallow landsliding on the northern hillslopes of

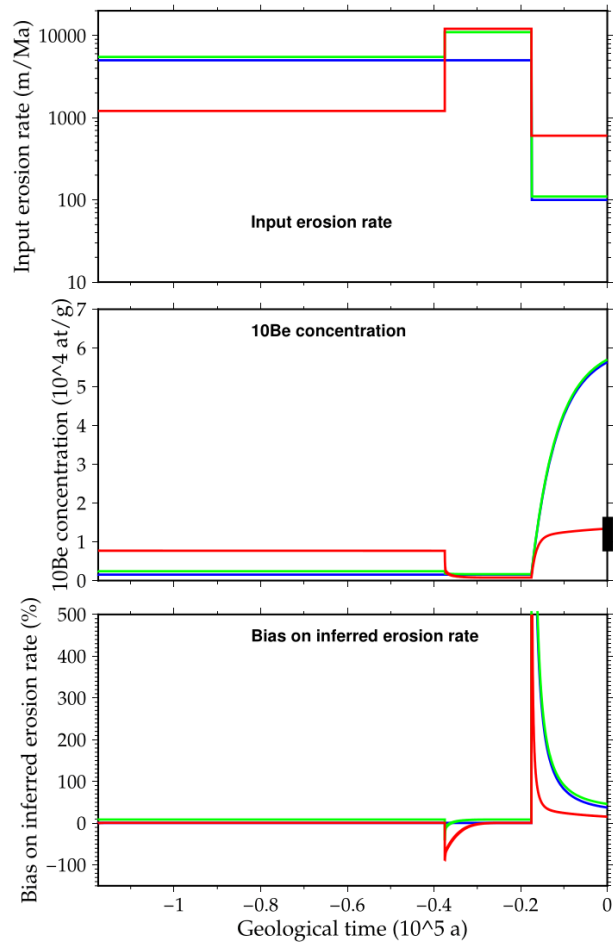
651 Chaitén volcano ($42^{\circ}48'24.48''\text{S}$, $72^{\circ}37'30.61''\text{W}$). All UAV footage was obtained in 2018 using

652 a Sensefly eBee RTK (a,c) and DJI Mavic Pro (b). Numbers in (c) refer to contour-parallel

653 profiles through recent landslides.

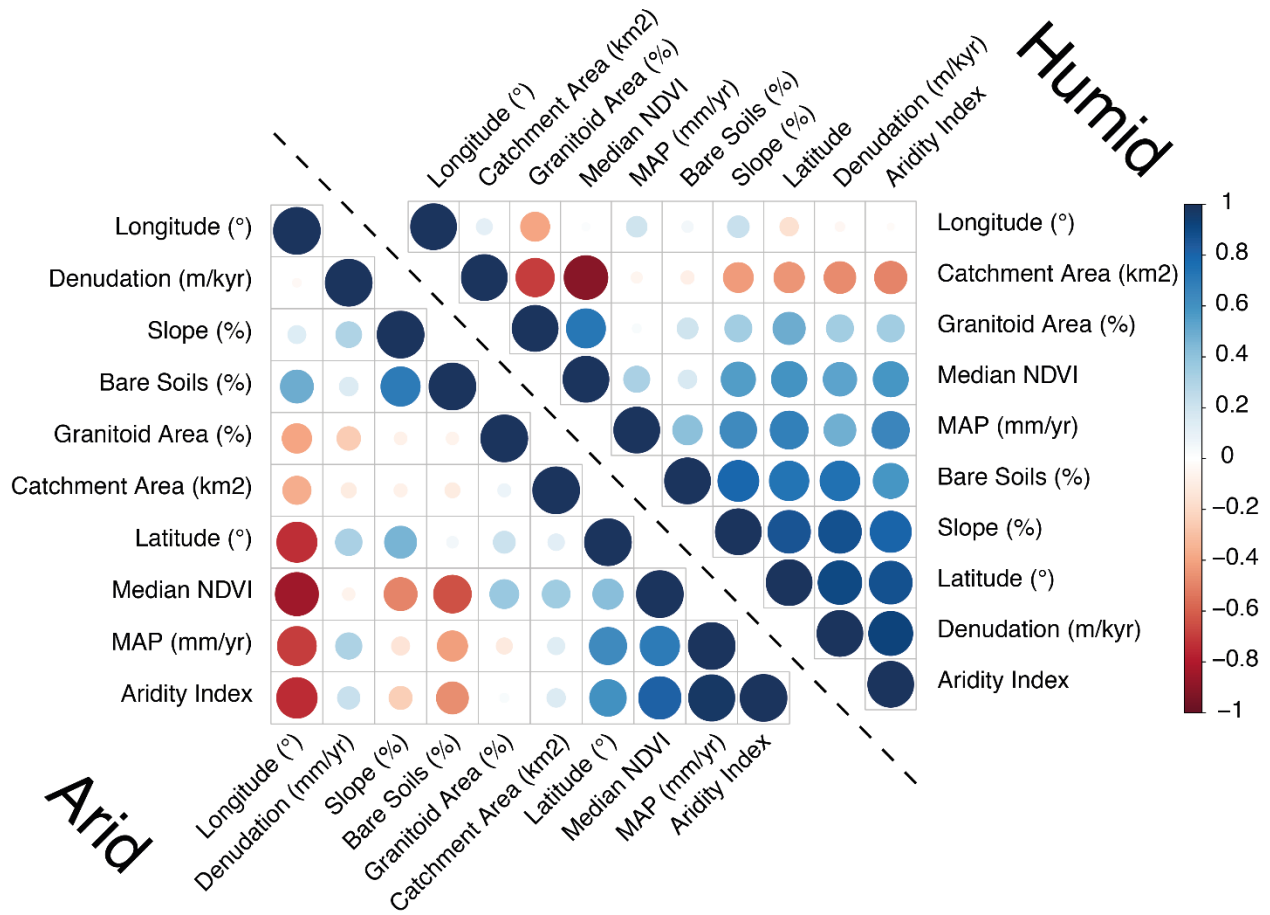
654

655



656

657 Supplementary Figure 3. Test of a possible glacial erosion inheritance. We test if our denudation
 658 rates could be biased by higher erosion during last glacial maximum and thus be less than
 659 estimated, for example 0.1 m/kyr rather than 0.5 mm/a. We test 3 scenarios with 2 pre-17.5 ka
 660 periods with higher erosion rates over 80 ka. Whatever these rates, the bias on the estimated
 661 erosion rate using riverine ^{10}Be is low. For the red scenario, that predicts the correct ^{10}Be
 662 concentration (see black rectangle in the middle panel), the bias is < 10 % even if the last glacial
 663 maximum corresponded to erosion rates as high as 10 m/kyr. The ^{10}Be production rate is 10
 664 at/g/yr in each case and the ^{10}Be concentration is calculated using muon and neutron productions
 665 ⁸⁹ as well as radioactive decay.



667
 668 Supplementary Figure 4. Correlation plot illustrating multicollinearities between denudation and
 669 hydroclimatic, geological, and spatial predictors grouped for arid (AI<1) and humid (AI>1) areas
 670 in Chile⁴²⁻⁴⁴. New data is included.

671



672

673 Supplementary Figure 5. 360° panorama view of Caleta Gonzalo catchment (42°34'06.91''S,
674 72°37'42.60''). highlighting dense Patagonian coastal temperate rainforest closely connected to
675 the Pacific Ocean. Drone footage was acquired using a DJI Phantom 4 by Benjamin Sotomayor in
676 03/2022.

677

678 **Supplementary References**

- 679 1. Bonan, G. B. Forests and Climate Change: Forcings, Feedbacks, and the Climate Benefits
680 of Forests. *Science (1979)* **320**, 1444–1449 (2008).
- 681 2. Canadell, J. G. & Raupach, M. R. Managing forests for climate change mitigation. *Science*
682 *(1979)* **320**, 1456–1457 (2008).
- 683 3. Sidle, R. C. & Ochiai, H. Land Use and Global Change. in *Landslides: Processes,*
684 *Prediction, and Land Use* 1–76 (2006).
- 685 4. Korup, O., McSaveney, M. J. & Davies, T. R. H. Sediment generation and delivery from
686 large historic landslides in the Southern Alps, New Zealand. *Geomorphology* **61**, 189–207
687 (2004).
- 688 5. Hilton, R. G., Meunier, P., Hovius, N., Bellingham, P. J. & Galy, A. Landslide impact on
689 organic carbon cycling in a temperate montane forest. *Earth Surface Processes and*
690 *Landforms* **36**, 1670–1679 (2011).
- 691 6. Mohr, C. H., Korup, O., Ulloa, H. & Iroumé, A. Pyroclastic Eruption Boosts Organic
692 Carbon Fluxes Into Patagonian Fjords. *Global Biogeochemical Cycles* **31**, 1626–1638
693 (2017).
- 694 7. Starke, J., Ehlers, T. A. & Schaller, M. Latitudinal effect of vegetation on erosion rates
695 identified along western South America. *Science (1979)* **367**, 1358–1361 (2020).
- 696 8. Langbein, W. B. & Schumm, S. A. Yield of sediment in relation to mean annual
697 precipitation. *Transactions, American Geophysical Union* **39**, 1076 (1958).
- 698 9. Acosta, V. T. *et al.* Effect of vegetation cover on millennial-scale landscape denudation
699 rates in East Africa. *Lithosphere* **7**, 408–420 (2015).
- 700 10. Schmid, M., Ehlers, T. A., Werner, C., Hickler, T. & Fuentes-Espoz, J. P. Effect of
701 changing vegetation and precipitation on denudation - Part 2: Predicted landscape
702 response to transient climate and vegetation cover over millennial to million-year
703 timescales. *Earth Surface Dynamics* **6**, 859–881 (2018).
- 704 11. Vanacker, V. *et al.* Restoring dense vegetation can slow mountain erosion to near natural
705 benchmark levels. *Geology* **35**, 303 (2007).
- 706 12. Turner, M. G., Romme, W. H., Gardner, R. H., O'neill, R. v & Kratz, T. K. *A revised*
707 *concept of landscape equilibrium: Disturbance and stability on scaled landscapes.*
708 *Landscape Ecology* vol. 8 (1993).
- 709 13. Granger, D. E. & Schaller, M. Cosmogenic Nuclides and Erosion at the Watershed Scale.
710 *Elements* **10**, 369–373 (2014).
- 711 14. Schaefer, J. M. *et al.* Cosmogenic nuclide techniques. *Nature Reviews Methods Primers* **2**,
712 18 (2022).
- 713 15. Myers, N., Mittermeier, R. A., Mittermeier, C. G., da Fonseca, G. A. B. & Kent, J.
714 Biodiversity hotspots for conservation priorities. *Nature* **403**, 853–858 (2000).

- 715 16. Keith, H., Mackey, B. G. & Lindenmayer, D. B. Re-evaluation of forest biomass carbon
716 stocks and lessons from the world's most carbon-dense forests. *Proc Natl Acad Sci U S A*
717 **106**, 11635–11640 (2009).
- 718 17. DellaSala, D. A. *Temperate and Boreal Rainforests of the World: Ecology and*
719 *Conservation*. (Island Press/Center for Resource Economics, 2011). doi:10.5822/978-1-
720 61091-008-8.
- 721 18. Alaback, P. Comparative ecology of temperate rainforests of the Americas along
722 analogous climatic gradients. *Revista Chilena de Historia Natural* **64**, 399–412 (1991).
- 723 19. de La Barrera, F., Reyes-Paecke, S. & Meza, L. Landscape analysis for rapid ecological
724 assessment of relocation alternatives for a devastated city. *Revista Chilena de Historia*
725 *Natural* **84**, 181–194 (2011).
- 726 20. Moreno, P. I. *et al.* Radiocarbon chronology of the last glacial maximum and its
727 termination in northwestern Patagonia. *Quaternary Science Reviews* **122**, 233–249 (2015).
- 728 21. de Porras, M. E. *et al.* Postglacial vegetation, fire and climate dynamics at Central Chilean
729 Patagonia (Lake Shaman, 44°S). *Quaternary Science Reviews* **50**, 71–85 (2012).
- 730 22. Torrejón, F., Cisternas, M., Alvial, I. & Torres, L. Colonial timber felling consequences of
731 the alerce forests in Chiloé, southern Chile (18th and 19th centuries). *Magallania (Punta*
732 *Arenas)* **39**, 75–95 (2011).
- 733 23. Urbina, M. X. Análisis histórico-cultural del alerce en la Patagonia septentrional
734 occidental, Chiloé, siglos XVI al XIX. *Magallania (Punta Arenas)* **39**, 57–73 (2011).
- 735 24. Buma, B. *et al.* Emergent freeze and fire disturbance dynamics in temperate rainforests.
736 *Austral Ecology* **44**, 812–826 (2019).
- 737 25. Markgraf, V. & Huber, U. M. Late and postglacial vegetation and fire history in Southern
738 Patagonia and Tierra del Fuego. *Palaeogeography, Palaeoclimatology, Palaeoecology*
739 **297**, 351–366 (2010).
- 740 26. Sommerfeld, A. *et al.* Patterns and drivers of recent disturbances across the temperate
741 forest biome. *Nature Communications* **9**, (2018).
- 742 27. Morales, B. *et al.* A comparative machine learning approach to identify landslide
743 triggering factors in northern Chilean Patagonia. *Landslides* **18**, 2767–2784 (2021).
- 744 28. Sepúlveda, S. A., Serey, A., Lara, M., Pavez, A. & Rebolledo, S. Landslides induced by
745 the April 2007 Aysén fjord earthquake, Chilean Patagonia. *Landslides* **7**, 483–492 (2010).
- 746 29. Korup, O., Seidemann, J. & Mohr, C. H. Increased landslide activity on forested hillslopes
747 following two recent volcanic eruptions in Chile. *Nature Geoscience* **2–8** (2019)
748 doi:10.1038/s41561-019-0315-9.
- 749 30. Parra, E., Mohr, C. & Korup, O. Predicting Patagonian Landslides: Roles of Forest Cover
750 and Wind Speed. (2021) doi:10.1029/2021GL095224.
- 751 31. Mohr, C. H., Manga, M., Wang, C. Y. & Korup, O. Regional changes in streamflow after
752 a megathrust earthquake. *Earth and Planetary Science Letters* **458**, 418–428 (2017).
- 753 32. Veblen, T. Forest development in tree-fall gaps in the temperate rain forest of Chile. *Natl.*
754 *Geogr. Res.* **1**, 162–183 (1985).
- 755 33. Sernageomin. Mapa geológico de Chile: versión digital. *Publicación Geología Digital* vol.
756 **4** 25 (2003).
- 757 34. Zomer, R. J. *et al.* *Trees and Water: Smallholder Agroforestry on Irrigated Lands in*
758 *Northern India*. IWMI report (2007).
- 759 35. Codilean, A. T. *et al.* OCTOPUS: an open cosmogenic isotope and luminescence
760 database. *Earth System Science Data* **10**, 2123–2139 (2018).

- 761 36. Müller Schmied, H. *et al.* Sensitivity of simulated global-scale freshwater fluxes and
762 storages to input data, hydrological model structure, human water use and calibration.
763 *Hydrology and Earth System Sciences* **18**, 3511–3538 (2014).
- 764 37. Hansen, M. C. *et al.* High-Resolution Global Maps of 21st-Century Forest Cover Change.
765 *Science (1979)* **342**, 850–853 (2013).
- 766 38. Burdis, A. J. Denudation rates derived from spatially-averaged cosmogenic nuclide
767 analysis in Nelson/Tasman catchments, South Island, New Zealand. (Victoria University
768 of Wellington, 2014).
- 769 39. Bellingham, M. F. Climatic effects on rapid chemical and physical denudation rates
770 measured with cosmogenic nuclides in the Ōhau catchment, New Zealand. (Victoria
771 University of Wellington, 2020).
- 772 40. Moon, S. *et al.* Climatic control of denudation in the deglaciated landscape of the
773 Washington Cascades. *Nature Geoscience* **4**, 469–473 (2011).
- 774 41. Roering, J. J., Perron, J. T. & Kirchner, J. W. Functional relationships between denudation
775 and hillslope form and relief. *Earth and Planetary Science Letters* **264**, 245–258 (2007).
- 776 42. Carretier, S. *et al.* Erosion in the Chilean Andes between 27°S and 39°S: tectonic, climatic
777 and geomorphic control. *Geological Society, London, Special Publications* **399**, 401–418
778 (2015).
- 779 43. Carretier, S. *et al.* Differences in ¹⁰Be concentrations between river sand, gravel and
780 pebbles along the western side of the central Andes. *Quaternary Geochronology* **27**, 33–
781 51 (2015).
- 782 44. Tolorza, V. Magnitude and Dynamics of catchment erosion in the Biobío River Basin.
783 (Universidad de Chile, 2015).
- 784 45. Mishra, A. K., Placzek, C. & Jones, R. Coupled influence of precipitation and vegetation
785 on millennial-scale erosion rates derived from ¹⁰Be. *PLOS ONE* **14**, e0211325 (2019).
- 786 46. Alvarez-Garretón, C. *et al.* The CAMELS-CL dataset: catchment attributes and
787 meteorology for large sample studies – Chile dataset. *Hydrology and Earth System
788 Sciences Discussions* 1–40 (2018) doi:10.5194/hess-2018-23.
- 789 47. Urrutia-Jalabert, R., Malhi, Y. & Lara, A. The Oldest, Slowest Rainforests in the World?
790 Massive Biomass and Slow Carbon Dynamics of Fitzroya cupressoides Temperate Forests
791 in Southern Chile. *PLOS ONE* **10**, e0137569 (2015).
- 792 48. Mohr, C. H., Manga, M., Wang, C., Kirchner, J. W. & Bronstert, A. Shaking water out of
793 soil. *Geology* **43**, 207–210 (2015).
- 794 49. Hales, T. C. & Roering, J. J. Climatic controls on frost cracking and implications for the
795 evolution of bedrock landscapes. *Journal of Geophysical Research* **112**, F02033 (2007).
- 796 50. Carretier, S. *et al.* Slope and climate variability control of erosion in the Andes of central
797 Chile. *Geology* **41**, 195–198 (2013).
- 798 51. Sidle, R. C. A Conceptual Model of Changes in Root Cohesion in Response to Vegetation
799 Management. *Journal of Environmental Quality* **20**, 43–52 (1991).
- 800 52. Vorpahl, P., Dislich, C., Elsenbeer, H., Märker, M. & Schröder, B. Biotic controls on
801 shallow translational landslides. *Earth Surface Processes and Landforms* **38**, 198–212
802 (2013).
- 803 53. Spors, S. Suicidal forests ? – Modelling biomass surcharge as a potential landslide driver
804 in temperate rainforests of Chilean Patagonia. (Universität Potsdam, 2021).
- 805 54. Larsen, I. J., Montgomery, D. R. & Korup, O. Landslide erosion controlled by hillslope
806 material. *Nature Geoscience* **3**, 247–251 (2010).

- 807 55. Amundson, R., Heimsath, A., Owen, J., Yoo, K. & Dietrich, W. E. Hillslope soils and
808 vegetation. *Geomorphology* **234**, 122–132 (2015).
- 809 56. Fosdick, J. C., Grove, M., Hourigan, J. K. & Calderón, M. Retroarc deformation and
810 exhumation near the end of the Andes, southern Patagonia. *Earth and Planetary Science*
811 *Letters* **361**, 504–517 (2013).
- 812 57. Andrić-Tomašević, N. *et al.* Quantifying Tectonic and Glacial Controls on Topography in
813 the Patagonian Andes (46.5°S) From Integrated Thermochronometry and Thermo-
814 Kinematic Modeling. *Journal of Geophysical Research: Earth Surface* **126**, (2021).
- 815 58. Georgieva, V. *et al.* Tectonic control on rock uplift, exhumation, and topography above an
816 oceanic ridge collision: Southern Patagonian Andes (47°S), Chile. *Tectonics* **35**, 1317–
817 1341 (2016).
- 818 59. Gray, A. N., Whittier, T. R. & Harmon, M. E. Carbon stocks and accumulation rates in
819 Pacific Northwest forests: Role of stand age, plant community, and productivity.
820 *Ecosphere* **7**, 1–19 (2016).
- 821 60. Stephenson, N. L. *et al.* Rate of tree carbon accumulation increases continuously with tree
822 size. *Nature* **507**, 90–93 (2014).
- 823 61. Frith, N. v. *et al.* Carbon export from mountain forests enhanced by earthquake-triggered
824 landslides over millennia. *Nature Geoscience* **11**, 772–776 (2018).
- 825 62. Smith, R. W., Bianchi, T. S., Allison, M., Savage, C. & Galy, V. High rates of organic
826 carbon burial in fjord sediments globally. *Nature Geoscience* **8**, 450–453 (2015).
- 827 63. Singer, B. S., Ackert, R. P. & Guillou, H. 40Ar/39Ar and K-Ar chronology of Pleistocene
828 glaciations in Patagonia. *Geological Society of America Bulletin* **116**, 434 (2004).
- 829 64. Cembrano, J., Hervé, F. & Lavenu, A. The Liquiñe Ofqui fault zone: a long-lived intra-arc
830 fault system in southern Chile. *Tectonophysics* **259**, 55–66 (1996).
- 831 65. Pepin, E., Carretier, S., Guyot, J. L. & Escobar, F. Specific suspended sediment yields of
832 the Andean rivers of Chile and their relationship to climate, slope and vegetation.
833 *Hydrological Sciences Journal* **55**, 1190–1205 (2010).
- 834 66. Carretier, S. *et al.* Review of erosion dynamics along the major N-S climatic gradient in
835 Chile and perspectives. *Geomorphology* **300**, 45–68 (2018).
- 836 67. Lal, D. Cosmic ray labeling of erosion surfaces: in situ nuclide production rates and
837 erosion models. *Earth and Planetary Science Letters* **104**, 424–439 (1991).
- 838 68. von Blanckenburg, F. & Willenbring, J. K. Cosmogenic Nuclides: Dates and Rates of
839 Earth-Surface Change. *Elements* **10**, 341–346 (2014).
- 840 69. Kohl, C. P. & Nishiizumi, K. Chemical isolation of quartz for measurement of in-situ -
841 produced cosmogenic nuclides. *Geochimica et Cosmochimica Acta* **56**, 3583–3587 (1992).
- 842 70. von Blanckenburg, F., Belshaw, N. S. & O’Nions, R. K. Separation of ⁹Be and
843 cosmogenic ¹⁰Be from environmental materials and SIMS isotope dilution analysis.
844 *Chemical Geology* **129**, 93–99 (1996).
- 845 71. Wilcken, K. M. *et al.* SIRIUS Performance: ¹⁰Be, ²⁶Al and ³⁶Cl measurements at
846 ANSTO. *Nuclear Instruments and Methods in Physics Research Section B: Beam*
847 *Interactions with Materials and Atoms* **455**, 300–304 (2019).
- 848 72. Nishiizumi, K. *et al.* Absolute calibration of ¹⁰Be AMS standards. *Nuclear Instruments*
849 *and Methods in Physics Research, Section B: Beam Interactions with Materials and*
850 *Atoms* **258**, 403–413 (2007).

- 851 73. Mudd, S. M., Harel, M.-A., Hurst, M. D., Grieve, S. W. D. & Marrero, S. M. The CAIRN
852 method: automated, reproducible calculation of catchment-averaged denudation rates from
853 cosmogenic nuclide concentrations. *Earth Surface Dynamics* **4**, 655–674 (2016).
- 854 74. Braucher, R., Merchel, S., Borgomano, J. & Bourlès, D. L. Production of cosmogenic
855 radionuclides at great depth: A multi element approach. *Earth and Planetary Science*
856 *Letters* **309**, 1–9 (2011).
- 857 75. Jarvis, A., Reuter, H. I., Nelson, A. & Guevara, E. Hole-filled SRTM for the globe
858 Version 4. *available from the CGIAR-CSI SRTM 90m Database* vol. 15
859 <http://srtm.csi.cgiar.org> (2008).
- 860 76. Stone, J. O. Air pressure and cosmogenic isotope production. *Journal of Geophysical*
861 *Research: Solid Earth* **105**, 23753–23759 (2000).
- 862 77. Compo, G. P. *et al.* The Twentieth Century Reanalysis Project. *Quarterly Journal of the*
863 *Royal Meteorological Society* vol. 137 1–28 (2011).
- 864 78. Codilean, A. T. Calculation of the cosmogenic nuclide production topographic shielding
865 scaling factor for large areas using DEMs. *Earth Surface Processes and Landforms* **31**,
866 785–794 (2006).
- 867 79. Zambrano-Bigiarini, M., Nauditt, A., Birkel, C., Verbist, K. & Ribbe, L. Temporal and
868 spatial evaluation of satellite-based rainfall estimates across the complex topographical
869 and climatic gradients of Chile. *Hydrology and Earth System Sciences* **21**, 1295–1320
870 (2017).
- 871 80. Zhao, Y. *et al.* Detailed dynamic land cover mapping of Chile: Accuracy improvement by
872 integrating multi-temporal data. *Remote Sensing of Environment* **183**, 170–185 (2016).
- 873 81. Zomer, R. J., Trabucco, A., Bossio, D. A. & Verchot, L. v. Climate change mitigation: A
874 spatial analysis of global land suitability for clean development mechanism afforestation
875 and reforestation. *Agriculture, Ecosystems and Environment* **126**, 67–80 (2008).
- 876 82. Gorelick, N. *et al.* Google Earth Engine: Planetary-scale geospatial analysis for everyone.
877 *Remote Sensing of Environment* **202**, 18–27 (2017).
- 878 83. Breiman, L. Random Forests. *Machine Learning* **45**, 5–32 (2001).
- 879 84. Liaw, A. & Wiener, M. Classification and Regression by randomForest. *R News* **2**, 18–22
880 (2002).
- 881 85. Strobl, C., Boulesteix, A. L., Kneib, T., Augustin, T. & Zeileis, A. Conditional variable
882 importance for random forests. *BMC Bioinformatics* **9**, 1–11 (2008).
- 883 86. Larsen, I. J. *et al.* Rapid soil production and weathering in the Southern Alps, New
884 Zealand. *Science* **343**, 637–40 (2014).
- 885 87. Carretier, S. *et al.* A note on 10 Be-derived mean erosion rates in catchments with
886 heterogeneous lithology: examples from the western Central Andes. *Earth Surface*
887 *Processes and Landforms* **40**, 1719–1729 (2015).
- 888 88. Kober, F. *et al.* Complex multiple cosmogenic nuclide concentration and histories in the
889 arid Rio Lluta catchment, northern Chile. *Earth Surface Processes and Landforms* **34**,
890 398–412 (2009).
- 891 89. Braucher, R. *et al.* Determination of muon attenuation lengths in depth profiles from in
892 situ produced cosmogenic nuclides. *Nuclear Instruments and Methods in Physics*
893 *Research Section B: Beam Interactions with Materials and Atoms* **294**, 484–490 (2013).
- 894
895